Submitted to Physical Review D

LBL-384
Preprint

COHERENT K^+D INTERACTIONS AT 12 GeV/c

A. Firestone, G. Goldhaber, D. Lissauer, and
G. H. Trilling

October 11, 1971

AEC Contract No. W-7405-eng-48

DISCLAIMER

LBL-384

COHERENT K^+D INTERACTIONS AT 12 GeV/c*

A. Firestone, G. Goldhaber, D. Lissauer, and G. H. Trilling

Department of Physics and Lawrence Berkeley Laboratory
University of California, Berkeley, California 94720

October 11, 1971

ABSTRACT

We have made a study of the coherent reactions $K^+d \to K^+\pi^+\pi^-d$ and $K^+d \to K^o\pi^+d$ at 12 GeV/c, using data obtained in the SLAC 82-inch bubble chamber. The cross sections for these two processes are 331±35 and 19±4 μb respectively. The reaction $K^+d \to K^+\pi^+\pi^-d$ is dominated by Q production in the $K\pi\pi$ system. The shape of the Q enhancement is nearly identical to that observed in the reaction $K^+p \to K^+\pi^+\pi^-p$ at similar energies. This result may be interpreted in terms of mixing between the strange members of the A_1 and B nonets. There are also an L signal at $M(K\pi\pi) \sim 1.72$ GeV and a d^* signal at $M(d\pi^+) \sim 2.2$ GeV. The L appears to be formed primarily in conjunction with the d^*, with the π^+ meson shared between the two of them. The reaction $K^+d \to K^o\pi^+d$ is dominated completely by $K^*(890)$ production.

I. INTRODUCTION

In this paper we present an analysis of the coherent reactions $K^+d \to K^+\pi^+\pi^-d$ and $K^+d \to K^0\pi^+d$ at 12 GeV/c, from data obtained with the SLAC 82-inch deuterium-filled bubble chamber. These reactions, in which the deuteron emerges intact in the final state, are particularly interesting in that the coherence acts as a filter in allowing only $I = 0$ non-spin-flip exchange at the deuteron vertex.

It has been suggested that the Q, as produced in hydrogen, for example in the reaction $K^+p \to K^+\pi^+\pi^-p$, has both $J^{PC} = 1^{++}$ and 1^{+-} components, where C is the charge conjugation quantum number of the neutral nonstrange members of the same nonet ($C = +1$ for the A_1 nonet and $C = -1$ for the B nonet).[1-3] Since the strange mesons are not eigenstates of C, a generalization of C called "unitary parity" has been introduced by Dothan, which is expected to hold for each entire nonet.[4] A particularly straightforward interpretation for two distinct $J^P = 1^+$ states is obtained from the quark model where the A_1 and B nonets are considered as the $^3P_1$ and $^1P_1$ $q\bar{q}$ states.[5]

Experimentally the evidence[6,7] that the Q enhancement consists of (at least) two distinct $J^P = 1^+$ states appears rather well established by now[8,9]: the Q_A at $M \approx 1.25$ GeV and Q_B at $M \approx 1.38$ GeV. The lower mass state, Q_A, may be the same object as the C(1240) meson observed in nondiffractive reactions.[10]

Two overlapping $J^P = 1^+$ K^* states, which decay into the same final state, $K\pi\pi$, may give rise to new phenomena. The states can mix[1] so that the physical states Q_A and Q_B are mixtures of the intrinsic states K_A and K_B belonging to the two distinct nonets. Thus one can define a mixing angle φ such that[11]:

$$Q_A = K_A \cos\varphi + K_B \sin\varphi$$

$$Q_B = -K_A \sin\varphi + K_B \cos\varphi \quad .$$

Furthermore, interference effects between the physical states Q_A and Q_B may also be present.[2] In the absence of mixing between these two components of the Q (exact SU_3 symmetry), and with the assumption of Pomeron exchange, the $J^{PC} = 1^{+-}$ component of the Q (i.e., Q_B) is expected to vanish in the coherent reaction in deuterium. Conversely the presence of Q_B in coherent production can be interpreted as evidence for the above mentioned K^* mixing effect. The work reported here includes the results of a search for these mixing effects, as well as a study of L and d^* production.

In Sec. II we discuss the beam, scanning, measuring, and separation techniques which were used to obtain the data sample of $K^+d \to K^+\pi^+\pi^-d$ events. In addition, ambiguity problems and our methods of handling them are discussed at length. In Sec. III we describe the general features of the reaction, and the cross-section determination is given. In Sec. IV the physics of the d^* enhancement is presented and in Sec. V the L meson data are discussed. Section VI deals with the Q enhancement and treats production mechanisms as well as decay properties. Section VII deals briefly with the companion coherent reaction $K^+d \to K^0\pi^+d$, and Sec. VIII presents the main conclusions of this study.

II. DATA SAMPLE

A. General Analysis

Approximately 500,000 photographs were taken in an exposure of the SLAC 82-inch bubble chamber to an rf-separated 12-GeV/c K^+ meson beam. Incident momentum resolution to within $\Delta p/p = \pm 0.2\%$ is achieved by using the known correlation between beam momentum and transverse position in the bubble chamber.[12] Through the use of a gas Čerenkov counter, pion contamination in the beam is reduced essentially to zero. On the average 8 K^+ mesons were incident in the chamber per pulse. The bubble chamber was filled with deuterium, but there was a hydrogen contamination of 4.5%.[13]

The film was scanned for events of the following topologies: (i) four-prongs with at least one stopping track, (ii) three-prongs, (iii) one- or two-prongs plus a vee. The events were measured on the LRL Flying-Spot Digitizer, and were reconstructed and kinematically fitted in the program SIOUX. Remeasurements were performed on conventional digitizing machines.

The odd-prong events are assigned a particle of zero momentum with suitable errors. For the deuteron hypotheses, i.e., $K^+d \rightarrow K^+\pi^+\pi^-d$ and $K^+d \rightarrow K^o\pi^+d$, this missing recoil deuteron is assigned momentum errors, $\Delta P_x = \Delta P_y = \pm 40$ MeV/c, and $\Delta P_z = \pm 50$ MeV/c. For the reactions with unseen spectator protons, e.g., $K^+d \rightarrow K^+\pi^+\pi^-pn$, the assigned errors are $\Delta P_x = \Delta P_y = \pm 30$ MeV/c, and $\Delta P_z = \pm 40$ MeV/c. These errors reflect the fact that a proton of momentum less than 70 MeV/c leaves no visible track in the bubble chamber, while a deuteron must have a minimum momentum of 110 MeV/c to be visible.

B. Identification of $K^+\pi^+\pi^-d$ Events

The four-pronged events which satisfy the four-constraint kinematic hypothesis, $K^+d \rightarrow K^+\pi^+\pi^-d$, with χ^2 less than 20 are accepted. To judge the reliability of this kinematic fit we have studied all the four-pronged events which fit the corresponding one-constraint hypothesis, $K^+d \rightarrow K^+\pi^+\pi^-pn$. We find that 97% of the four prongs which fit the four-constraint hypothesis also fit the corresponding one-constraint hypothesis. Figure 1 shows the invariant mass of the proton, neutron combination, M(p,n), for all events making this one-constraint fit. The shaded region represents that subsample which fits the four-constraint deuteron hypothesis as well. The sharp spike at the minimum M(p,n) is attributable entirely to the four-constraint events. This spike is centered at about 1.879 GeV (the sum of the proton and neutron rest masses), and has a width of less than 2 MeV. Figure 2 shows the distribution in cos θ, the angle in the laboratory frame between the proton and neutron

for all one-constraint events. The shaded region again refers to the subsample also making the four-constraint fit. The spike at $\cos\theta = +1$, i.e., the proton and neutron traveling in the same direction, is attributable entirely to the events fitting the four-constraint hypothesis, $K^+d \rightarrow K^+\pi^+\pi^-d$.

In the three-prong events there is the problem of contamination from the tau decay of the incident K^+, i.e., $K^+ \rightarrow \pi^+\pi^+\pi^-$. All the three prongs which fit the tau hypothesis also fit the four-constraint deuteron hypothesis, $K^+d \rightarrow K^+\pi^+\pi^-d$. For all events which make the deuteron hypothesis we have deliberately misinterpreted the outgoing K^+ as a π^+, and have then calculated the resulting three "pion" effective mass from the measured momenta. The distribution in this mass is shown in Fig. 3. The spike at the K mass, due to the tau events, is very clean and an essentially complete separation is achieved by a cut at 560 MeV in this variable. This cut removes only a negligible number of $K^+\pi^+\pi^-d$ events.

In the three-pronged events, the hypothesis $K^+d \rightarrow K^+\pi^+\pi^-pn$, is underconstrained unless the unseen spectator proton is assigned a particular momentum. We have performed a one-constraint fit in which the proton is assigned a momentum of zero with errors as discussed earlier. All the three-pronged events which fit the four-constraint hypothesis, $K^+d \rightarrow K^+\pi^+\pi^-d$, also fit this one-constraint hypothesis, $K^+d \rightarrow K^+\pi^+\pi^-pn$. Figure 4 shows the distribution in M(p,n) for all events which fit this one-constraint hypothesis with the tau decays removed. The shaded region refers to the subsample which also fit the four-constraint deuteron hypothesis, $K^+d \rightarrow K^+\pi^+\pi^-d$, with χ^2 less than 10. The sharp spike at the minimum M(p,n) is here also attributable entirely to the four-constraint deuteron events. The depletion of events at M(p,n) ~ 1.9 GeV may be a consequence of the assignment of zero momentum to the unseen spectator.

In order to obtain a clean sample of $K^+d \rightarrow K^+\pi^+\pi^-d$ events we have restricted the sample to events with M(p,n) from the corresponding one-constraint

fit to be less than 1.886 GeV. This cut is of minor consequence in the four prongs, but was imposed there for consistency with the three prongs.

Figure 5 shows the deuteron momentum distribution for the complete sample of three prongs and four prongs. The shaded region represents the subsample of three-prong events. The distributions for the three- and four-pronged events match reasonably well with no apparent bias or loss of events. The sample of $K^+d \rightarrow K^+\pi^+\pi^-d$ events thus obtained is 5609 events, of which 70% are four-prongs.

C. The K^+-π^+ Ambiguity

With the above procedures we have identified the coherent events in which the deuteron remains intact and a $K^+\pi^+\pi^-$ is produced. Since the meson momenta typically average about 4 GeV/c, the kinematics are not significantly affected by the interchange of the K^+ and π^+. Thus 61% of the entire sample, i.e., 69% of the three prongs and 57% of the four prongs, are kinematically ambiguous between the two hypotheses, $K^+d \rightarrow K^+\pi^+\pi^-d$, and the same hypothesis with the K^+ and π^+ tracks interchanged. Because of the high momenta involved, bubble density measurements are not capable of separating K^+ from π^+ mesons.

For events in which the two ambiguous solutions have a difference in chisquare greater than three, we have selected the solution with the lower χ^2. This reduces the ambiguous sample to 46% of the entire sample, i.e., 65% of the three prongs and 36% of the four prongs. Small chisquare differences between ambiguous fits often reflect measurement errors rather than real kinematic information. Furthermore, routine selection of the lower χ^2 solution may introduce a distinct bias into the data. In the three prongs, in particular, since the recoil particle has zero momentum in the initial approximation, the energy equation is most nearly balanced when the particle with the highest momentum is made the heavier, i.e., the K^+. Thus the choice of lower χ^2 is

in fact the choice of calling the highest momentum particle the K^+, and this choice is a bias towards low $K\pi\pi$ masses. Therefore, for the events with $\Delta\chi^2 < 3$ we have plotted in all one-dimensional histograms both solutions, each with a weight of 1/2. We have also tried an alternative procedure for treating the events with $\Delta\chi^2 < 3$, which preferentially selects $K^*(890)$ or $K^*(1420)$ solutions.[14] This alternative procedure was used in selecting solutions which are plotted in two-dimensional scatter plots.

The problem introduced by this K^+-π^+ ambiguity does not affect all kinematic regions of the data. In particular, when the π^+ is backward in the center-of-mass frame, i.e., slow in the laboratory, there is no ambiguity. Thus the d^* events may be studied with no ambiguity problem. The K^+-π^+ ambiguity limits the detail with which one can study the shape of the Q mass spectrum, since the two solutions have $K\pi\pi$ masses differing by typically 30 MeV. Thus, narrow structure might be reduced in significance, although the general shape of the Q would be unaffected. This problem also prevents an accurate determination of the $K^*\pi$ vs $K\rho$ decay branching ratios of the Q from our data. This is so because an event with a correctly assigned $M(K^+\pi^-)$ in the $K^*(890)$ peak contributes to a peak in the ρ region of $\pi^+\pi^-$ mass if the wrong solution is chosen; and moreover the reverse is also true.[15] Consequently we do not quote any $K^*\pi$ or $K\rho$ decay branching ratios of the Q, nor do we perform a detailed Dalitz plot spin-parity analysis.

III. GENERAL FEATURES OF THE $K^+\pi^+\pi^-d$ FINAL STATE

We have determined the cross section for the reaction $K^+d \rightarrow K^+\pi^+\pi^-d$ by normalizing our data to the K^+d total cross section at 12 GeV/c,[16] and correcting for the following effects: (1) the topological dependence of scanning efficiencies, (2) measurement efficiencies, and (3) hydrogen contamination in the bubble chamber. The resulting cross section is 331 ± 35 μb, where the quoted

uncertainty reflects both the statistics and our estimate of the systematic error, which is about 10%.

In Fig. 6 we show the distribution in $d\sigma/dt$ vs t for all $K^+d \rightarrow K^+\pi^+\pi^-d$ events. The data exhibit an approximate exponential form, $\frac{d\sigma}{dt} \propto e^{at}$ with $a = 25\pm2$ $(GeV/c)^{-2}$. The small dip in the very forward direction can be attributed to the effects of the Chew-Low boundary.

Figure 7 shows the distribution in $M(K\pi\pi)$ for all the events. The reaction is dominated by Q production, but there is some evidence for an L signal at a $K\pi\pi$ mass of about 1.7 GeV. In its gross features the Q mass peak appears very similar to the Q peak seen in hydrogen experiments, particularly the high-energy high-statistics K^+p experiments. The central value of the entire Q is about 1.3 GeV and the full width is about 300 MeV, and there is a sharp drop in the distribution at a mass of about 1.3 GeV. This is discussed in detail in Sec. VI.

Figure 8 shows the Chew-Low plot, $M^2(K\pi\pi)$ vs -t, for all the $K^+d \rightarrow K^+\pi^+\pi^-d$ events. The Q enhancement is produced primarily at very low $|t|$ values. The Chew-Low boundary cuts into the Q mass peak at values of $|t|$ less than or equal to 0.008 $(GeV/c)^2$, and has very little effect on the shape of the Q mass spectrum.

In Figs. 9 through 14 we show the two-body mass distributions; $M(K^+d)$, $M(K^+\pi^+)$, $M(K^+\pi^-)$, $M(\pi^+\pi^-)$, $M(d\pi^+)$ and $M(d\pi^-)$ respectively. The distribution in $M(K^+d)$ shows no evidence for any structure. The distribution in $M(K^+\pi^+)$ is concentrated at low mass since it reflects the low mass $K\pi\pi$ enhancement. The low mass excess in the $M(d\pi^-)$ distribution reflects the dynamics of Q decay. There is no evidence for any appreciable d^{*o} production. The distribution in $M(K^+\pi^-)$ is dominated by the $K^*(890)$, but there is evidence for $K^*(1420)$ production as well. The distribution in $M(\pi^+\pi^-)$ shows a ρ signal above the background, and the distribution in $M(d\pi^+)$ shows a clear d^* signal at the low-

mass end. As pointed out earlier, an incorrect resolution of the $K^+\pi^+$ ambiguity problem will result in a real $K^*(890)$ enhancement appearing as an apparent enhancement in the ρ region of the $\pi^+\pi^-$ mass. Therefore caution should be observed in interpreting the enhancement in the $M(\pi^+\pi^-)$ distribution as due entirely to actual ρ production.

In Fig. 15 we show the two-dimensional correlation plot: $M^2(K\pi\pi)$ vs $M^2(d\pi^+)$. The Q enhancement appears as the horizontal band and the d^* enhancement as the vertical band. The d^* band is populated over the range with $M^2(K\pi\pi) < 10\ (GeV)^2$, and is particularly prominent in the overlap regions with the L and Q. Figure 15 shows that the L enhancement appears almost entirely within the d^* band, i.e., there is no evidence for an L signal with $M(d\pi^+) < 3$ GeV. This effect is discussed in detail in Secs. IV and V. In Fig. 16 we show the two-dimensional correlation plot $M(K^+\pi^-)$ vs $M(\pi^+d)$, in which the $K^*(890)$ and d^* bands are very clear.

IV. THE d^* ENHANCEMENT

The narrow enhancement at the low mass end of Fig. 13 is the d^* peak. We have fit this peak to a Breit-Wigner shape over a polynomial background and obtain parameters $M = 2206 \pm 20$ MeV and $\Gamma = 140 \pm 26$ MeV for the d^*. This mass is consistent with the sum of a nucleon mass and the mass of the $\Delta(1238)$. This d^* peak has been observed earlier and interpreted as arising from the production of a $\Delta(1238)$ resonance whose decay nucleon recombines with the spectator nucleon to re-form the deuteron.[17] Evidence for this interpretation in our data is shown in Fig. 17 which shows the distribution in $\cos\theta$ for the d^* events [$M(d\pi^+) < 2.5$ GeV], where θ is the polar angle in the Gottfried-Jackson frame for the d^* peak, i.e., θ is the angle between the incident deuteron and the final deuteron in the $(d\pi^+)$ rest frame. The strong forward peaking is not at all characteristic of the decay of a single resonance, since

it requires a very large number of partial waves.[17] In this discussion we use the symbol d^* to refer to the observed enhancement in the $M(d\pi^+)$ distribution.

Figure 18 shows the distribution in the polar angle in the Gottfried-Jackson frame for the $K^+\pi^-$ system for the $K^*(890)d^*$ events, i.e., the angle from incident K^+ to outgoing K^+ in the $K^+\pi^-$ rest frame. The distribution is consistent with that expected for a $J^P = 1^-$ state produced by pion exchange. Thus pion exchange at the meson vertex dominates d^* production. Figure 19 shows the same distribution as in Fig. 18, but for the $K^*(1420)$ d^* events. This distribution is characteristic of $J^P = 2^+$ $K\pi$ state produced by pion exchange.

If we assume the interpretation of the d^* as a $\Delta(1238)$ with subsequent nucleon recombination, produced by pion exchange to the incident K^+ vertex, then the suppression of the d^{*o} (Fig. 14) with respect to the d^{*++} (Fig. 13) is easily understood in terms of the two diagrams shown in Fig. 20. Although the Δ^- and Δ^{++} have the same SU_2 coupling to the nucleon vertex, the exotic $K^+\pi^+$ scattering in Fig. 20b (d^{*o}) is expected to be much smaller than the $K^+\pi^-$ scattering in Fig. 20a (d^{*++}).[18]

In Fig. 21 we show the distribution in $M(K^+\pi^-)$ for the d^* events [$M(d\pi^+) < 2.5$ GeV]. The distribution in $M(K^+\pi^-)$ recoiling against the d^* shows an enhanced $K^*(1420)$ relative to the $K^*(890)$ in comparison with the total sample. This $K^+\pi^-$ mass distribution against the d^* appears to be very similar to the $K^+\pi^-$ mass distribution against the Δ^{++} in the hydrogen reaction $K^+p \to K^+\pi^+\pi^-p$.

Figures 22a and b show the distributions in $d\sigma/dt^*$ vs t^*, where $t^* = |t' - t'_{min}|$, t' is the square of the four-momentum transfer from the incident deuteron to the final $(d\pi^+)$ system, and t'_{min} is the kinematic limit evaluated at the center of the relevant K^* resonance, for the reactions $K^+d \to K^{*o}(890)d^{*++}$ and $K^{*o}(1420)d^{*++}$, respectively. The cross sections for the reactions $K^+d \to K^{*o}(890)d^{*++}$

and $K^{*o}(1420)d^{*++}$ are given in Table I. At 12 GeV/c the cross section for the reaction $K^+d \rightarrow K^{*o}(890)d^{*++}$ is about 20% of the cross section for the corresponding hydrogen reaction $K^+p \rightarrow K^{*o}(890)\Delta^{++}$ (Ref. 19). This can be compared to the result of Werner et al., who find that in K^- interactions at 5.5 GeV/c, the cross section for the reaction $K^-d \rightarrow \overline{K^{*o}}(890)d^{*o}$ is only 7% of the cross section for the reaction $K^-n \rightarrow \overline{K^{*o}}(890)\Delta^-$.[18] However in the K^-d interaction at 12 GeV/c, the cross section for d^{*o} production is not significantly different than that for d^{*++} production.[19a]

V. THE L ENHANCEMENT

In Fig. 15 (Sec. III) we showed the two-dimensional correlation plot, $M^2(K\pi\pi)$ vs $M^2(d\pi^+)$, with the surprising result that, in contrast to the Q, the L enhancement was seen almost entirely within the d^* band; and is, in fact, totally contained in the region with $M(d\pi^+) < 3$ GeV. In Fig. 23 we show the $K\pi\pi$ mass distribution for events with $M(d\pi^+)$ in the d^* region [$M(d\pi^+) < 2.5$ GeV]. Although some Q signal remains, this distribution is dominated by the L enhancement. We have fit this distribution in the region $1.5 \text{ GeV} < M(K\pi\pi) < 2.2$ GeV to a Breit-Wigner shape with polynomial background, and obtain the best fit parameters for the L: $M = 1730 \pm 20$ MeV and $\Gamma = 210 \pm 30$ MeV.

We have investigated the possibility that the absence of an L enhancement outside the d^* region might be caused by an incorrect resolution of the $K^+\pi^+$ ambiguity problem. Thus, for all ambiguous events we have chosen that solution with $M(K\pi\pi)$ closest to 1.75 GeV, and have plotted $M(K\pi\pi)$ for all ambiguous events thus resolved. There is no significant L signal above background even with this maximally enhancing procedure for $M(d\pi^+) > 3$ GeV. In addition, we have examined the distribution in $M(K^+\pi^-)$ for those events with $M(K\pi\pi)$ in the L region, using this maximally enhancing procedure; and, outside the d^* region, we find no evidence for a $K^*(1420)$ peak. Thus we conclude that the L signal is largely confined to the d^* region.

We have investigated the possibility that the L is a kinematical reflection

of the combined effects of the d^* decay angular distribution (Fig. 17) and the $K^*(1420)$. We have performed a Monte Carlo calculation, which uses the experimental d^* decay angular distribution, as well as the experimental d^* production angular distribution as fixed quantities, and which calculates the expected distribution in $M(K^*(1420)\pi)$. The results show an enhancement in the region of the L, which is significantly broader than the observed L signal (Fig. 23). Thus we conclude that the observed L signal is not consistent with a simple kinematical reflection of the d^* decay.

In Fig. 24 we show the distribution in $M(K^+\pi^-)$ for all the events in the d^* region with the L selected [1.6 GeV < $M(K\pi\pi)$ < 1.9 GeV]. The distribution is dominated by $K^*(890)$ and $K^*(1420)$. Even with d^* selection the L has a substantial background which may be due in part to the tail of the Q which would contain $K^*(890)\pi$. Therefore, in order to obtain information on the decay modes of the L, we have taken the distribution shown in Fig. 24 and subtracted from it the distribution in $M(K^+\pi^-)$ from control regions on either side of the L [1.45 GeV < $M(K\pi\pi)$ < 1.6 GeV and 1.9 GeV < $M(K\pi\pi)$ < 2.05 GeV]. This distribution is shown in Fig. 25. The data are consistent with entirely $K^*(1420)\pi$ decay of the L. However, a $K^*(890)\pi$ decay mode of the L is possible and we determine the branching fraction $[\frac{L \to K^*(890)\pi}{L \to K^*(1420)\pi}]$ to be equal to 17±11%. This result cannot resolve the contradiction between Barbaro-Galtieri et al.,[20] who have claimed the decay of the L is 100% $K^*(1420)\pi$, and both Aguilar-Benitez et al. and Bartsch et al.[21] who find evidence for other decay modes of the L.

Figure 26 shows the distribution in $M(\pi^+\pi^-)$ for the L events with d^* selected. Although there is perhaps some ρ signal present we can make no reliable estimate of the branching ratio of L decaying into $K\rho$. The data are consistent with no $K\rho$ decay at all.

In conclusion, we emphasize the fact that the L is produced in a strong association with the d^*. A similar process occurs in hydrogen where the L

appears to be produced largely in conjunction with the Δ^{++} in the reaction $K^+p \rightarrow K^+\pi^+\pi^-p$.[22] An L produced in this manner does not accord with the assumption of Pomeron exchange and the Harari-Freund duality hypothesis which associates only background with the Pomeron in the cross channel (see Fig. 27a). It would appear that at these energies isoscalar exchange other than the Pomeron, e.g., f exchange, must be important at the deuteron vertex (see Fig. 27b).

VI. THE Q ENHANCEMENT

The motivation for the study of coherent production of the Q in deuterium is to isolate the $I = 0$ non-spin flip exchange. By comparison with Q production in hydrogen, where other exchanges are allowed, we may identify which exchange mechanisms give rise to various parts of the Q mass spectrum. In Fig. 28 we compare our $K\pi\pi$ mass spectrum with a sample of hydrogen data used by Firestone in his compilation of high-energy K^+p data.[23] The hydrogen data was normalized to the deuterium population between 1.1 GeV and 1.5 GeV. The striking feature of these two distributions is their similarity, including the structure characterized by the sharp drop at $M(K\pi\pi) \sim 1.3$ GeV.

The small differences between the hydrogen and deuterium distributions can be attributed to the following effects: (1) The shift of the leading edge of the deuterium distribution to lower mass than the hydrogen can be explained by the fact that the deuteron form factor enhances the population near the Chew-Low boundary; (2) the excess of hydrogen events near 1.4 GeV is due to the strong suppression of $K^*(1420)$ production in the deuterium, as discussed more quantitatively below; (3) the difference in background levels above the region of the Q, $M(K\pi\pi) > 1.5$ GeV, can be understood in terms of the effects of the deuteron form factor, the possible presence of processes which can only occur through deuteron breakup, and the fact that the hydrogen data is a compilation of momenta running from 7.3 to 12.7 GeV/c.

We have attempted to fit our distribution of $M(K\pi\pi)$ in the region of the Q to a single Breit-Wigner shape without background, and the results are shown in Fig. 29a. The fit is very poor with $\chi^2 = 72.3$ for 22 degrees of freedom. In Fig. 29b we show the same distribution but now fit to two incoherent Breit-Wigner forms without background. The fit is acceptable with $\chi^2 = 25.9$ for 19 degrees of freedom. The parameters of the two Breit-Wigners are $M_A = 1234 \pm 12$ MeV and $\Gamma_A = 188 \pm 21$ MeV for the lower Q (Q_A); and $M_B = 1368 \pm 18$ MeV and $\Gamma_B = 241 \pm 30$ MeV for the upper Q (Q_B); these values are in good agreement with the parameters obtained in a similar fit for the hydrogen data.[9] It should be emphasized that the above values are the result of a specific parametrization which was used to compare various $K\pi\pi$ mass distributions,[9] but do not necessarily represent the masses and widths of the actual physical states.

From the coherent reaction $K^+d \rightarrow K^o\pi^+d$ (to be discussed in Sec. VII), and from the $K^*(1420)$ decay branching ratios reported in the Particle Data Tables, we determine a maximum $K^*(1420)$ contribution to the Q of 15 events. This $K^*(1420)$ contribution to the Q enhancement in the coherent events is relatively less than even the small contribution determined in the hydrogen case.[7] Thus, one cannot interpret the upper Breit-Wigner of the Q as the $K^*(1420)$. This has been previously noted in hydrogen production by Firestone,[9] Barnham et al.,[8] and Ferbel.[24]

The data indicate that the high mass portion of the Q enhancement, Q_B, produced coherently off a deuteron in this experiment, is as pronounced as in hydrogen; we interpret this fact as evidence that the entire Q enhancement is produced largely by $I = 0$ non-spin-flip exchange, which is most likely the Pomeron. The simplest explanation of this effect is essentially a maximal mixing between the two K^*'s, K_A and K_B, to produce the two physical states, Q_A and Q_B. The mixing angle, φ, defined in Sec. I, would have to be of the order of 45^o. A similar conclusion was recently reached by Garfinkel et al., using 9 GeV/c K^+d data.[25]

In Fig. 30 we show the distribution $d\sigma/dt'$ vs t' for the Q events only [$M(K\pi\pi) < 1.5$ GeV]. The distribution has been fit to an exponential form, $d\sigma/dt' = Ae^{Bt'}$ where $B = 29 \pm 1$ $(GeV/c)^{-2}$. This slope is consistent with that expected from a slope of about 8 $(GeV/c)^{-2}$ from the hydrogen Q data, combined with a slope of about 20 obtained from the average behavior of the deuteron form factor for the region $|t| < 0.1$ $(GeV/c)^2$; i.e., that region where the Q data is concentrated.

We have analyzed the Q as a function of $M(K\pi\pi)$, using the following five mass bins: 1.0-1.1 GeV, 1.1-1.2 GeV, 1.2-1.3 GeV, 1.3-1.4 GeV, and 1.4-1.5 GeV. Figures 31 through 33 each show the distribution of a particular angle in these five $M(K\pi\pi)$ intervals, plotted as parts a, b, c, d, and e respectively. In each case $K^*(890)$ events have been selected. In Fig. 31 we show the distribution in $\cos\theta$, where θ is the polar angle in the Gottfried-Jackson frame of the $K^*(890)$; i.e., the angle between the incident and final K^+ mesons in the $K^+\pi^-$ rest frame. The distributions are all largely $\cos^2\theta$. This is consistent with the commonly accepted interpretation of the Q as a $J^P = 1^+$ system, produced by Pomeron exchange, which decays mainly by S-wave into $K^*(890)\pi$, and where the spin of the $K^*(890)$ is aligned such that $m_J = 0$ along the incident direction.

Figure 32 shows the distributions in the polar angle N in the Gottfried-Jackson frame of the normal to the $K\pi\pi$ decay plane, i.e., the angle between the incident K^+ direction and the normal in the $K\pi\pi$ rest frame. The distributions are largely $\sin^2 N$, as expected for a $J^P = 1^+$ object, produced by Pomeron exchange, which has its spin aligned such that $m_J = 0$ along the beam direction.

In Fig. 33 we show the distributions in the cosine of the polar angle of the Q in the Gottfried-Jackson frame; i.e., the angle between the incident K^+ direction and the outgoing K^* direction in the $K\pi\pi$ rest frame. The distributions

are not consistent with isotropy, in that there is both a $\cos^2 K^*$ component and a forward-backward asymmetry in the distributions in Fig. 33. If we temporarily ignore the biases in these distributions due to the K^+-π^+ ambiguity problem and accept them at face value, then the most natural explanation of the $\cos^2 K^*$ component is the interference between the dominant S-wave decay of the Q with a small D-wave decay of the $J^P = 1^+$ Q into $K^*(890)\pi$. Furthermore, the asymmetry may be attributed to the interference of the dominant S-wave decay with a small $J^P = 0^-$ or $J^P = 2^-$ component of the Q, which decayed via P-wave into $K^*(890)\pi$. The Illinois Group has reported a substantial $J^P = 0^-$ component under the predominantly $J^P = 1^+$ A_1 meson,[26] and perhaps a similar effect is occurring in the Q. However, the non-isotropic components of the distributions of Fig. 33 may be due to contamination from $K\rho$ decay of the Q and incorrect resolution of the $K^+\pi^+$ ambiguity problem. The $K\rho$ and $K^*(890)\pi$ kinematic overlap region is large for the $K\pi\pi$ mass in the Q region, and no clean separation is possible. Thus the interpretation of this angle is ambiguous. Because of the ambiguity problem this coherent reaction is not the most suitable one for probing the details of the spin structure of the Q, i.e., possible $J^P = 0^-$ or $J^P = 2^-$ components, or a possible D-wave decay of a $J^P = 1^+$ Q.

Evidence has been presented that the hypothesis of t-channel helicity conservation is a better approximation to the data than s-channel helicity conservation for the diffractively produced A_1 meson[27] and Q meson.[28] Due to the effect of the deuteron form factor, the Q in this experiment is restricted to a region of very small momentum transfers, where the crossing angle between the helicity and Gottfried-Jackson frames is very small. Therefore we cannot distinguish significantly the predictions of s-channel or t-channel helicity conservation.

We have examined the Q-decay Dalitz plots as functions of $M(K\pi\pi)$, and note that even with the selection criteria maximally biased against a ρ signal,

some ρ signal remains, in particular at high values of $M(K\pi\pi)$. Moreover the bulk of the ρ signal lies in the crossover region with the $K^*(890)$. Because of the K^+-π^+ ambiguity problem, K^*-ρ interference, and their intimate overlap, no reliable estimate of the $K^*\pi$ vs Kρ branching ratio for the Q may be made in this experiment.

VII. THE REACTION $K^+d \to K^o\pi^+d$

We have also studied the coherent reaction $K^+d \to K^o\pi^+d$. Because of the excellent resolution from fitting the K^o decay, these events are highly constrained and may be separated reliably from all background with no ambiguities. We have obtained a sample of 133 events of this type with a cross section of 19±4 μb. This cross section has been corrected for the invisible decays of the K^o's as well as all the detection efficiencies outlined in Sec. II.

The Dalitz plot for this process is shown in Fig. 34. The reaction is dominated by $K^*(890)$ production with no substantial evidence for any other structure apart from a possible small $K^*(1420)$ signal. This can also be seen in the mass projections, $M(K^o\pi^+)$, $M(d\pi^+)$, and $M(dK^o)$ shown in Figs. 35, 36, and 37 respectively. From the distribution in $M(K^o\pi^+)$, shown in Fig. 35, we estimate an upper limit of 5 events in the $K^*(1420)$ region. After correcting for unseen K^o decays, Clebsch-Gordan coefficients, and the $K^*(1420)$ branching ratios as reported in the Particle Data Tables, we estimate the previously quoted 15 event upper limit of $K^*(1420)$ contribution to the Q enhancement in the reaction $K^+d \to K^+\pi^+\pi^-d$. We note that in the corresponding hydrogen reaction, $K^+p \to K^o\pi^+p$ at 9 GeV/c, the cross section for the reaction $K^+p \to K^*(1420)p$ was 37% of the cross section for the reaction $K^+p \to K^*(890)p$.[29] In deuterium, however, the $K^*(1420)$ cross section appears greatly suppressed and we place an upper limit on this ratio of 0.22.

VIII. CONCLUSIONS

In conclusion, the reaction $K^+d \to K^+\pi^+\pi^-d$ is dominated by Q production. The shape of the Q is very similar to that observed in hydrogen reactions, a shape not compatible with a single Breit-Wigner. The $K\pi\pi$ mass distribution in the region of the Q may be fit satisfactorily with two non-interfering Breit-Wigners with parameters $M_A = 1234\pm12$ MeV, $\Gamma_A = 188\pm21$ MeV, $M_B = 1368\pm18$ MeV, and $\Gamma_B = 241\pm30$ MeV. The contribution of the $K^*(1420)$ is extremely small; less than 15 events in this mass distribution. The Q is consistent with a predominantly $J^P = 1^+$ state, produced by Pomeron exchange, which decays via S-wave mainly into $K^*(890)\pi$. Furthermore, our data can be interpreted in terms of nearly maximal mixing between the two $J^P = 1^+$ K^*'s, K_A and K_B, to give the physical states Q_A and Q_B.

The L meson is produced primarily in conjunction with the d^* peak, with the π^+ shared between them. This production mechanism is not consistent with the assumption of Pomeron exchange and the Harari-Freund duality hypothesis.

The d^* enhancement is particularly striking in this reaction, and is interpreted as a Δ^{++} recombining with a neutron to give a deuteron and a π^+. The evidence for this interpretation is the decay angular distribution of the d^* which shows many partial waves to be present, and is what would be expected from on-shell π^+d elastic scattering.

We gratefully acknowledge the help of the SLAC accelerator operation group, and in particular we thank J. Murray, R. Gearhart, R. Watt, and the staff of the 82-inch bubble chamber for help with the exposure. We acknowledge the valuable support given by our scanning and programming staff, especially E. R. Burns, A. P. Habegger, and H. White and the staff of the Flying-Spot Digitizer.

REFERENCES

*Work supported by the U. S. Atomic Energy Commission.

1. R. Gatto, L. Maiani, and G. Preparata, Nuovo Cimento 39, 1192 (1965).

2. G. Goldhaber, Phys. Rev. Lett. 19, 976 (1967).

3. R. H. Dalitz, in Proceedings of the XIIIth International Conference on High-Energy Physics, Berkeley, 1966 (University of California Press, Berkeley, California, 1967), p. 215.

4. See for example, G. L. Kane, Phys. Rev. 156, 1738 (1967); also G. L. Kane and H. S. Mani, Phys. Rev. 171, 1533 (1968).

5. H. Lipkin, in Proceedings of the XIIIth International Conference on High-Energy Physics, Berkeley, 1966 (University of California Press, Berkeley, California, 1967).

6. G. Goldhaber, A. Firestone, and B. C. Shen, Phys. Rev. Lett. 19, 972 (1967).

7. G. Alexander, A. Firestone, G. Goldhaber, and D. Lissauer, Nucl. Phys. B13, 503 (1969).

8. K. W. J. Barnham et al., Nucl. Phys. B25, 49 (1970).

9. A. Firestone, The Q Region of $K\pi\pi$ Mass, in Experimental Meson Spectroscopy, ed. by C. Baltay and A. H. Rosenfeld (Columbia University Press, New York, 1970), p. 229.

10. R. Armenteros et al., Phys. Lett. 9, 207 (1964).

11. E. W. Colglazier and J. L. Rosner, Nucl. Phys. B27, 349 (1971).

12. S. Flatté, Lawrence Radiation Laboratory, Berkeley, Group A Memo 664 (1966).

13. R. D. Watt, Stanford Linear Accelerator Center, private communication.

14. Details of this procedure are given in D. Lissauer (Ph.D. thesis), Lawrence Radiation Laboratory Report UCRL-20644 (1971), unpublished.

15. T. Ferbel, R. Holmes, P. Slattery, and B. Werner, University of Rochester preprint UR-875-304 (1970).

16. W. Galbraith et al., Phys. Rev. 138, B913 (1965).

17. Evidence for the interpretation of the d^* effect as Δ production with recombination was first presented by M. A. Abolins, Phys. Rev. Lett. 15, 125 (1965) and I. Butterworth et al., Phys. Rev. Lett. 15, 500 (1965).

18. B. Werner et al., Nucl. Phys. B23, 37 (1970).

19. J. Berlinghieri et al., Nucl. Phys. B8, 333 (1968).

19a. D. Denegri et al., Johns Hopkins University preprint JHU-7014 Rev. (1971).

20. A. Barbaro-Galtieri et al., Phys. Rev. Lett. 22, 1207 (1969).

21. M. Aguilar-Benitez et al., Phys. Rev. Lett. 25, 54 (1970) and J. Bartsch et al., Phys. Lett. 33B, 186 (1970).

22. The strong association of L production with the Δ^{++} in the reaction $K^+p \rightarrow K^+\pi^+\pi^-p$ can be seen clearly in Fig. 10 of C.-Y. Chien, in Experimental Meson Spectroscopy, ed. by C. Baltay and A. H. Rosenfeld (Columbia University Press, New York, 1970), p. 289; and Fig. 1 of Ref. 15.

23. See Fig. 24 of Ref. 9.

24. T. Ferbel, University of Rochester preprint UR-875-337, has proposed a model which purports to explain the Q_B as an interference effect between the Q and the $K^*(1420)$. This suggestion is unlikely firstly because there is insufficient $K^*(1420)$, and secondly because Q_B has a decay angular distribution characteristic of $J^P = 1^+$ and not $J^P = 2^+$.

25. A. F. Garfinkel et al., Phys. Rev. Lett. 26, 1505 (1971).

26. A. Ascoli et al., Phys. Rev. Lett. 25, 962 (1970) and D. V. Brockway (Ph.D. thesis), University of Illinois Report No. COO-1195-197 (1970), unpublished.

27. Illinois-Genova-Hamburg-Milano-Saclay-Harvard-Toronto-Wisconsin Collaboration, Phys. Rev. Lett. 26, 929 (1971).

28. Aachen-Berlin-Bonn-CERN-Cracow-Heidelberg-London-Vienna Collaboration, Phys. Lett. 34B, 160 (1971).

29. V. G. Lind et al., Nucl. Phys. B14, 1 (1969).

Table I. Cross sections.

The cross sections for the specific reactions are obtained from the indicated mass cuts with no background subtraction.

	Events	σ (μb)
$K^+d \to K^+\pi^+\pi^-d$	5606	331±35
$K^+d \to Q^+d$, $Q^+ \to K^+\pi^+\pi^-$(a)	3604	213±21
$K^+d \to L^+d$, $L^+ \to K^+\pi^+\pi^-$(b)	306	~ 18
$K^+d \to K^+\pi^-d^{*++}$, $d^{*++} \to d\pi^+$(c)	1020	60±6
$K^+d \to K^{*o}(890)d^{*++}$, $d^{*++} \to d\pi^+$, $K^{*o}(890) \to K^+\pi^-$(d)	328	19±3
$K^+d \to K^{*o}(1420)d^{*++}$, $d^{*++} \to d\pi^+$, $K^{*o}(1420) \to K^+\pi^-$(e)	204	~ 12
$K^+d \to K^o\pi^+d$	133	19±4
$K^+d \to K^{*+}(890)d$	60	9±2
$K^+d \to K^{*+}(1420)d$	< 13	< 2

(a) Q: 1.0 GeV < $M(K\pi\pi)$ < 1.5 GeV.

(b) L: 1.6 GeV < $M(K\pi\pi)$ < 1.9 GeV; $M(d\pi^+)$ < 2.5 GeV.

(c) d^*: 2.0 GeV < $M(d\pi^+)$ < 2.5 GeV.

(d) $K^*(890)$: 0.84 GeV < $M(K^+\pi^-)$ < 0.94 GeV.

(e) $K^*(1420)$: 1.3 GeV < $M(K^+\pi^-)$ < 1.5 GeV.

FIGURE CAPTIONS

Fig. 1. M(p,n) for the four-prong events $K^+d \to K^+\pi^+\pi^-pn$. The shaded region refers to the subsample $K^+d \to K^+\pi^+\pi^-d$.

Fig. 2. Cos θ(p,n) for the four-prong events $K^+d \to K^+\pi^+\pi^-pn$. The shaded region refers to the subsample $K^+d \to K^+\pi^+\pi^-d$.

Fig. 3. M(3"π") for the three-prong events consistent with $K^+d \to K^+\pi^+\pi^-d$.

Fig. 4. M(p,n) for the three-prong events $K^+d \to K^+\pi^+\pi^-pn$. The shaded region refers to the subsample $K^+d \to K^+\pi^+\pi^-d$.

Fig. 5. Deuteron momentum distribution in the laboratory for all $K^+d \to K^+\pi^+\pi^-d$ events. The shaded region refers to the subsample of three-prong events.

Fig. 6. $d\sigma/dt$ vs t for all $K^+d \to K^+\pi^+\pi^-d$ events.

Fig. 7. M($K\pi\pi$) for all $K^+d \to K^+\pi^+\pi^-d$ events.

Fig. 8. Chew-Low plot $M^2(K\pi\pi)$ vs -t for all $K^+d \to K^+\pi^+\pi^-d$ events.

Fig. 9. M(K^+d) for all $K^+d \to K^+\pi^+\pi^-d$ events.

Fig. 10. M($K^+\pi^+$) for all $K^+d \to K^+\pi^+\pi^-d$ events.

Fig. 11. M($K^+\pi^-$) for all $K^+d \to K^+\pi^+\pi^-d$ events.

Fig. 12. M($\pi^+\pi^-$) for all $K^+d \to K^+\pi^+\pi^-d$ events.

Fig. 13. M($d\pi^+$) for all $K^+d \to K^+\pi^+\pi^-d$ events.

Fig. 14. M($d\pi^-$) for all $K^+d \to K^+\pi^+\pi^-d$ events.

Fig. 15. $M^2(K\pi\pi)$ vs $M^2(d\pi^+)$ for all $K^+d \to K^+\pi^+\pi^-d$ events.

Fig. 16. M($K^+\pi^-$) vs M($d\pi^+$) for all $K^+d \to K^+\pi^+\pi^-d$ events.

Fig. 17. Distribution in cos θ_{d^*} for the d^* events.

Fig. 18. Distribution in cos θ_{K^*} for the $K^*(890)d^*$ events.

Fig. 19. Distribution in cos θ_{K^*} for the $K^*(1420)d^*$ events.

Fig. 20. Diagrams for d^{*++} and d^{*o} production through Δ^{++} and Δ^- production.

Fig. 21. M($K^+\pi^-$) for the d^* events.

Fig. 22. $d\sigma/dt^*$ vs t^* for (a) the reaction $K^+d \to K^{*o}(890)d^{*++}$ and (b) the reaction $K^+d \to K^{*o}(1420)d^{*++}$.

Fig. 23. $M(K\pi\pi)$ for the d^* events.

Fig. 24. $M(K^+\pi^-)$ for the d^* events with L also selected.

Fig. 25. $M(K^+\pi^-)$ for the d^* events with L selected and control regions on either side of the L subtracted off.

Fig. 26. $M(\pi^+\pi^-)$ for the d^* events with L also selected.

Fig. 27. Diagrams for L production through Pomeron or f exchange.

Fig. 28. $M(K\pi\pi)$ for all $K^+d \to K^+\pi^+\pi^-d$ events with the d^* removed. The dashed histogram is the distribution in $M(K\pi\pi)$ from Ref. 23 renormalized to the population in this experiment between 1.1 and 1.5 GeV.

Fig. 29. $M(K\pi\pi)$ for all $K^+d \to K^+\pi^+\pi^-d$ events. The smooth curves refer to the results of fits to the hypotheses (a) a single Breit-Wigner shape, and (b) two incoherent Breit-Wigner forms.

Fig. 30. $d\sigma/dt'$ vs t' for the Q events [$M(K\pi\pi) < 1.5$ GeV].

Fig. 31. Distribution in cos θ as a function of $M(K\pi\pi)$, where θ is the polar angle in the Gottfried-Jackson frame.

Fig. 32. Distribution in cos N as a function of $M(K\pi\pi)$, where N is the normal to the $K\pi\pi$ decay plane in the $K\pi\pi$ rest frame.

Fig. 33. Distribution in cos K^* as a function of $M(K\pi\pi)$, where K^* is the polar angle of the $K^*(890)$ in the $K\pi\pi$ rest frame.

Fig. 34. Dalitz plot $M^2(K^o\pi^+)$ vs $M^2(\pi^+d)$ for the reaction $K^+d \to K^o\pi^+d$.

Fig. 35. $M(K^o\pi^+)$ for the reaction $K^+d \to K^o\pi^+d$.

Fig. 36. $M(\pi^+d)$ for the reaction $K^+d \to K^o\pi^+d$.

Fig. 37. $M(K^od)$ for the reaction $K^+d \to K^o\pi^+d$.

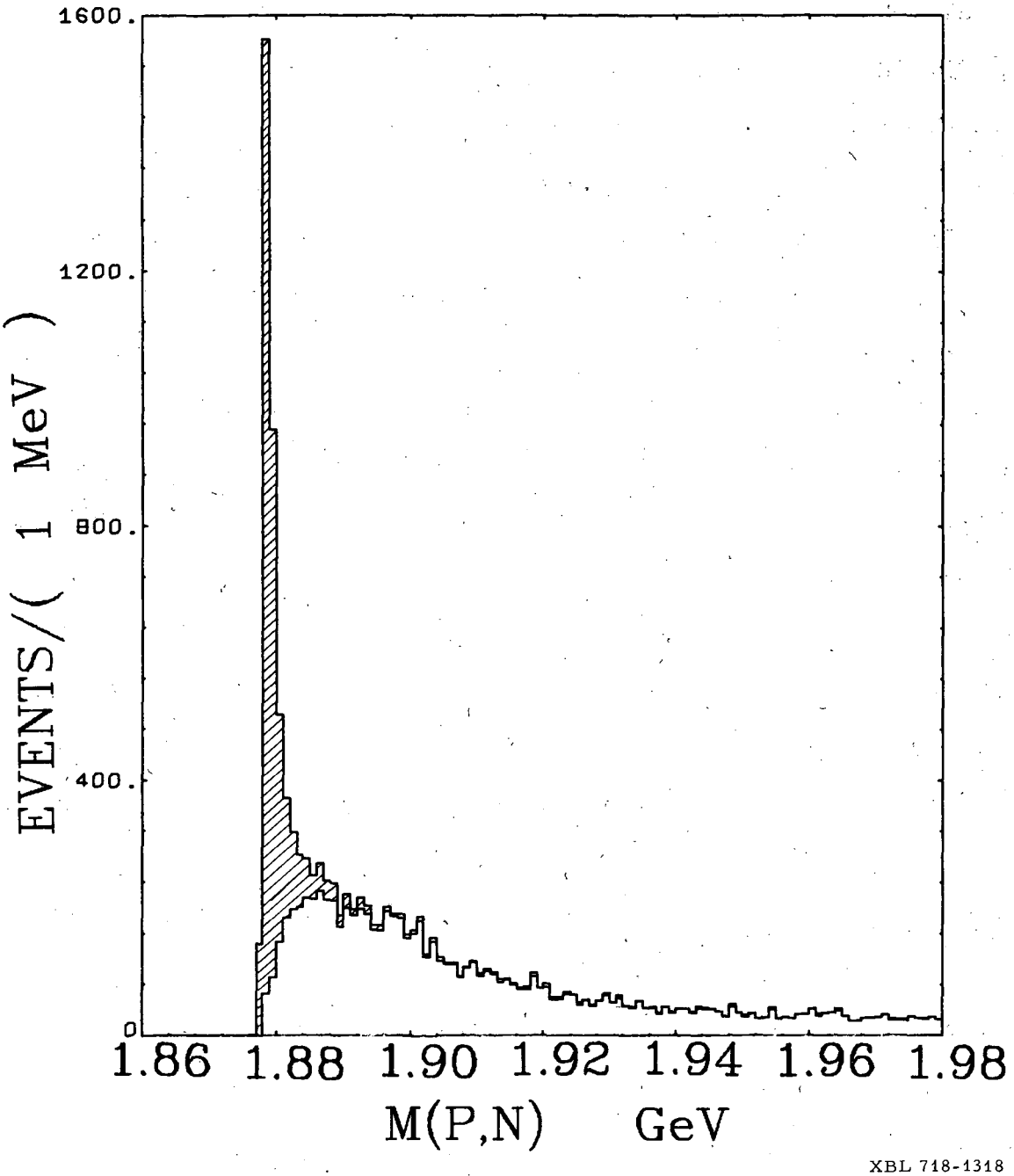
1600.
1200.
800.
400.
0
EVENTS/(1 MeV)
1.86 1.88 1.90 1.92 1.94 1.96 1.98
M(P,N) GeV
XBL 718-1318

Fig. 1

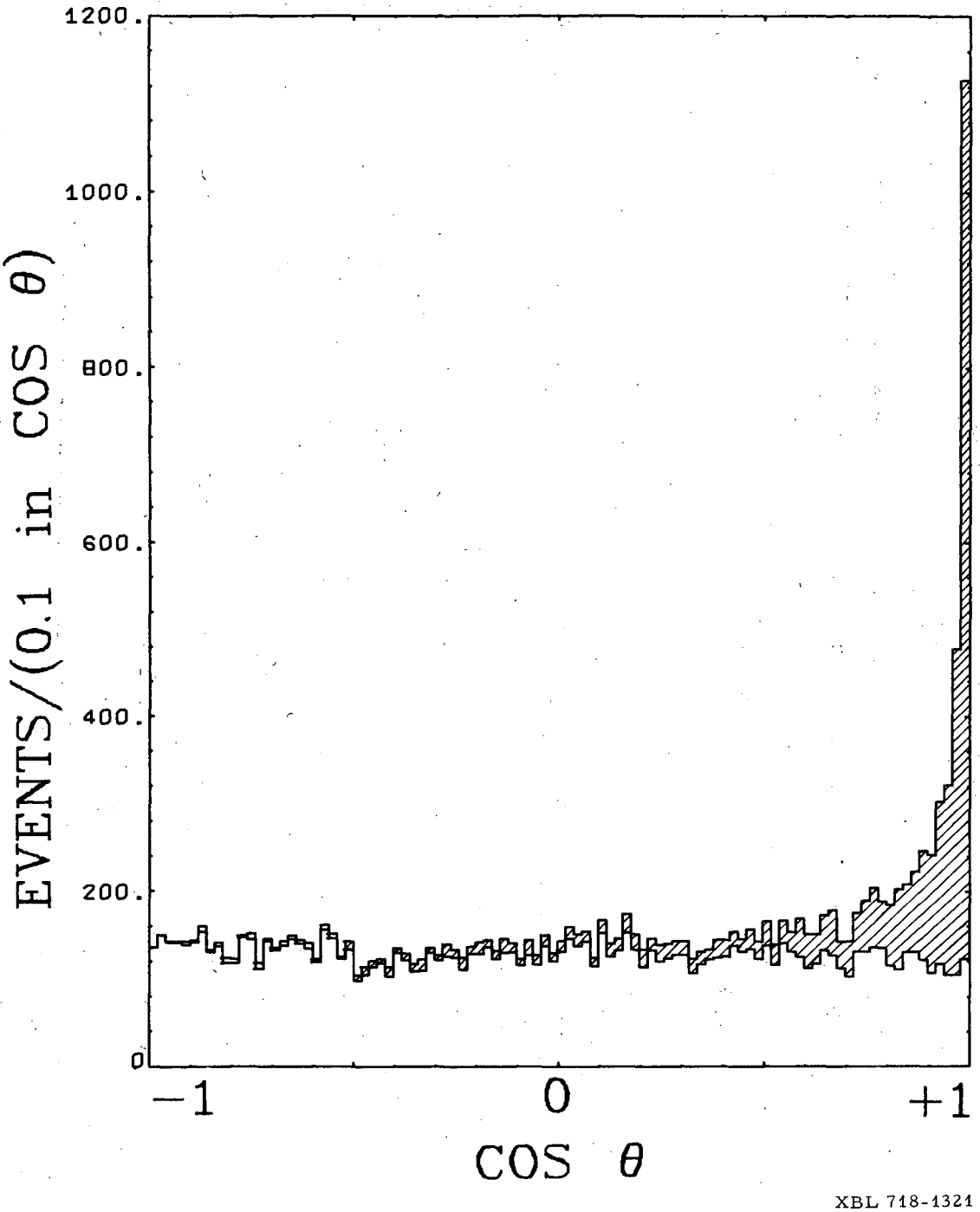

Fig. 2

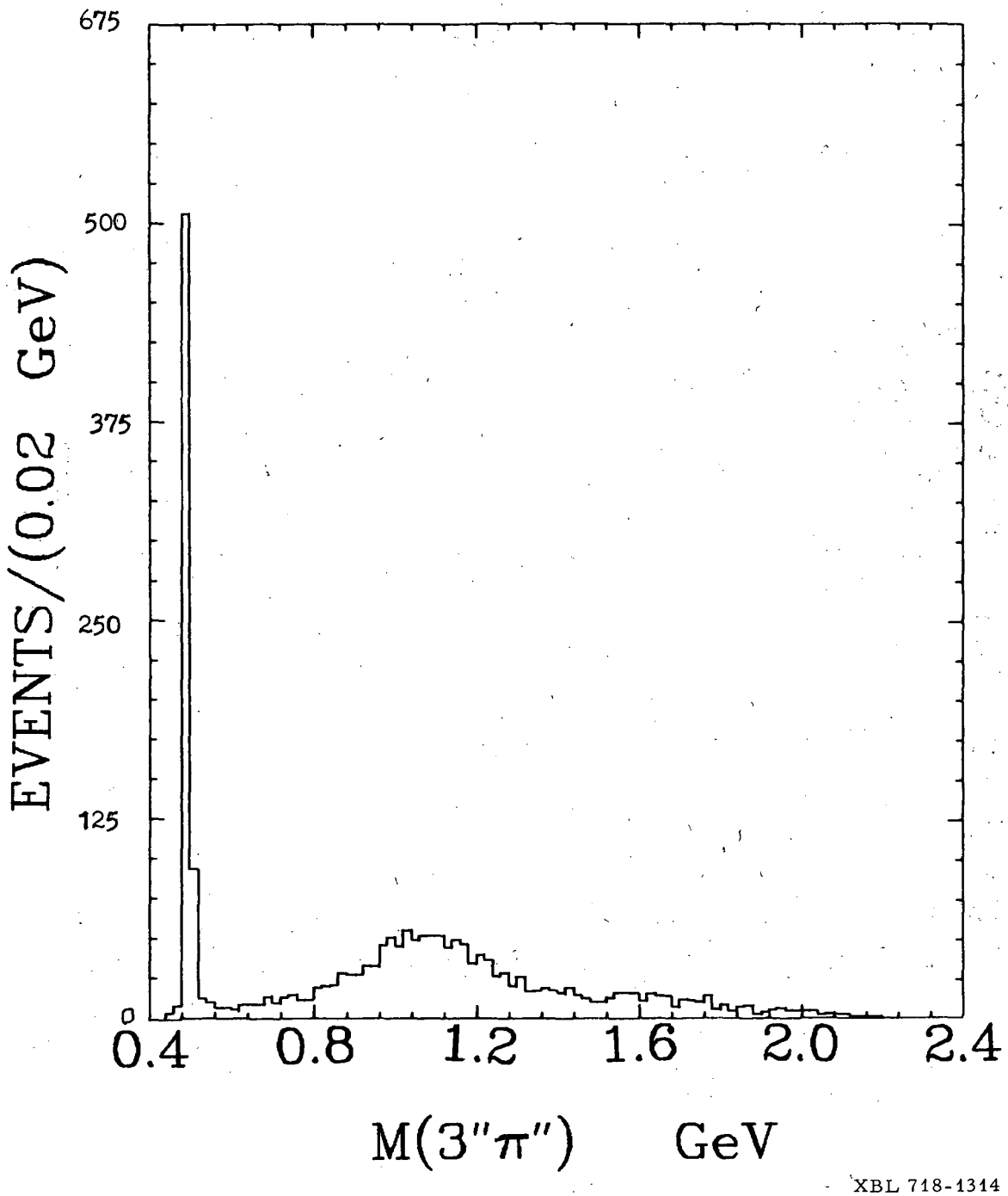
675
500
375
250
125
0
EVENTS/(0.02 GeV)
0.4
0.8
1.2
1.6
2.0
2.4
M(3"π") GeV
XBL 718-1314

Fig. 3

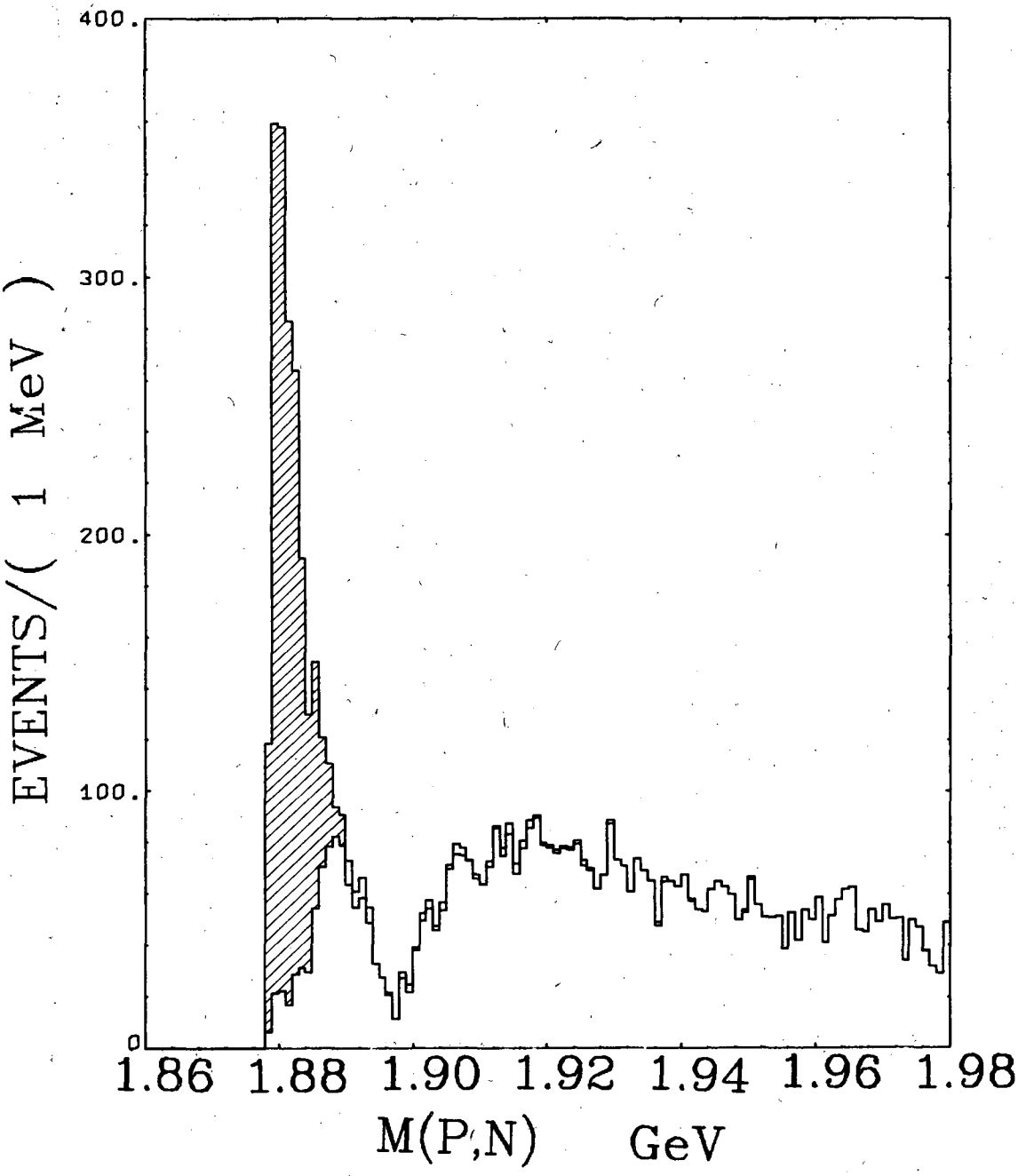

XBL 718-1312

Fig. 4

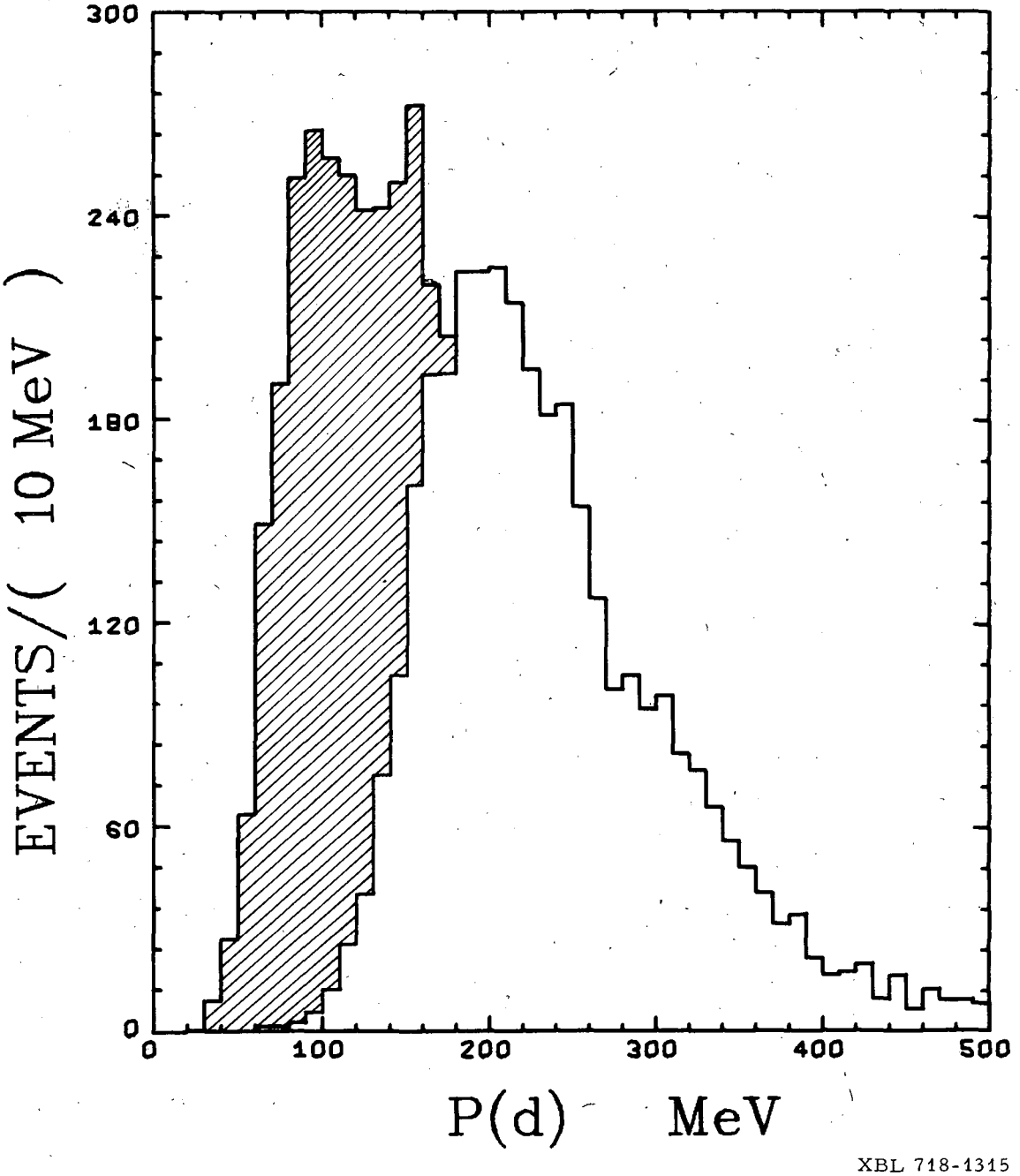
300
240
180
120
60
0
EVENTS/(10 MeV)
0
100
200
300
400
500
P(d) MeV
XBL 718-1315

Fig. 5

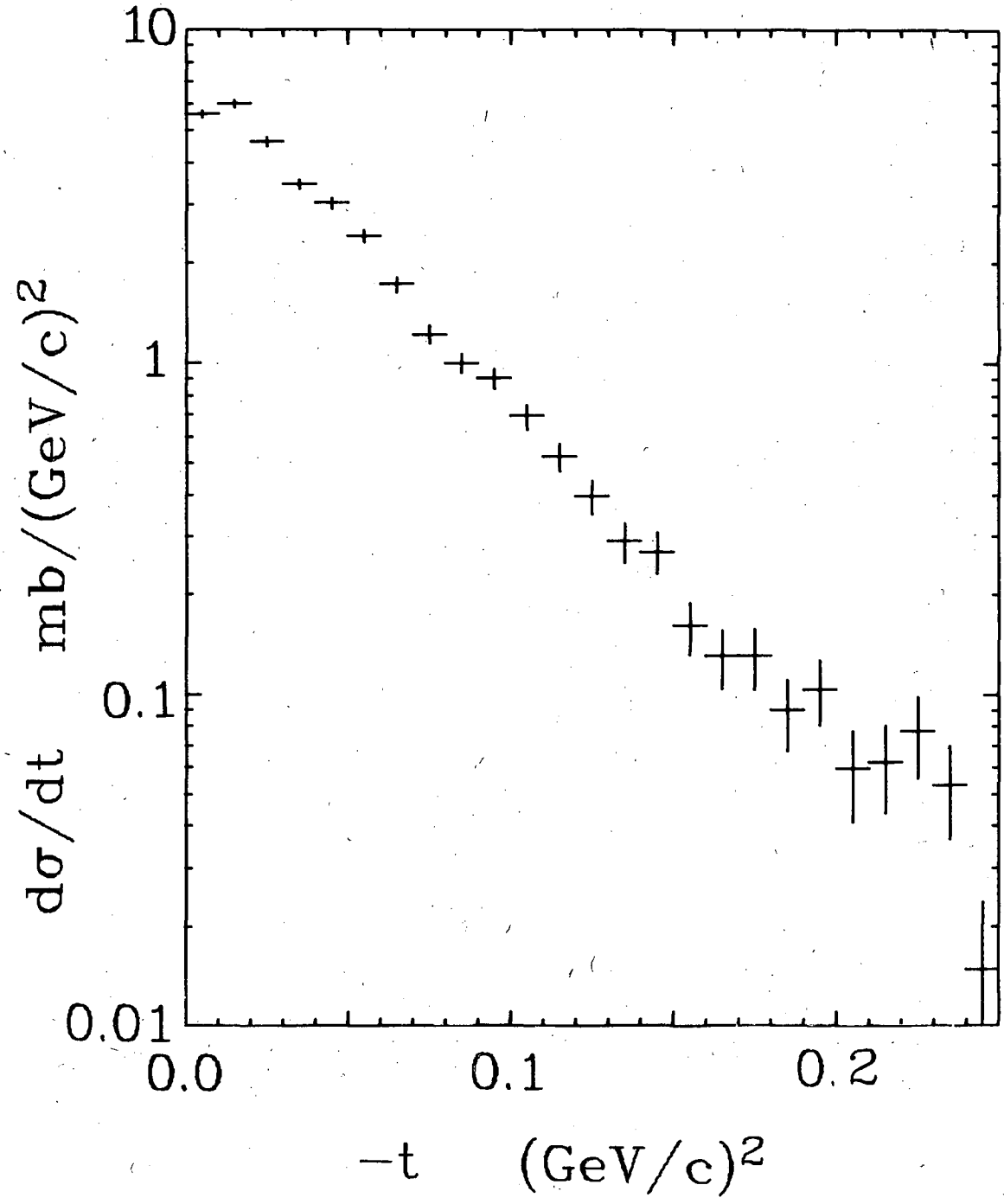

XBL 719-1349

Fig. 6

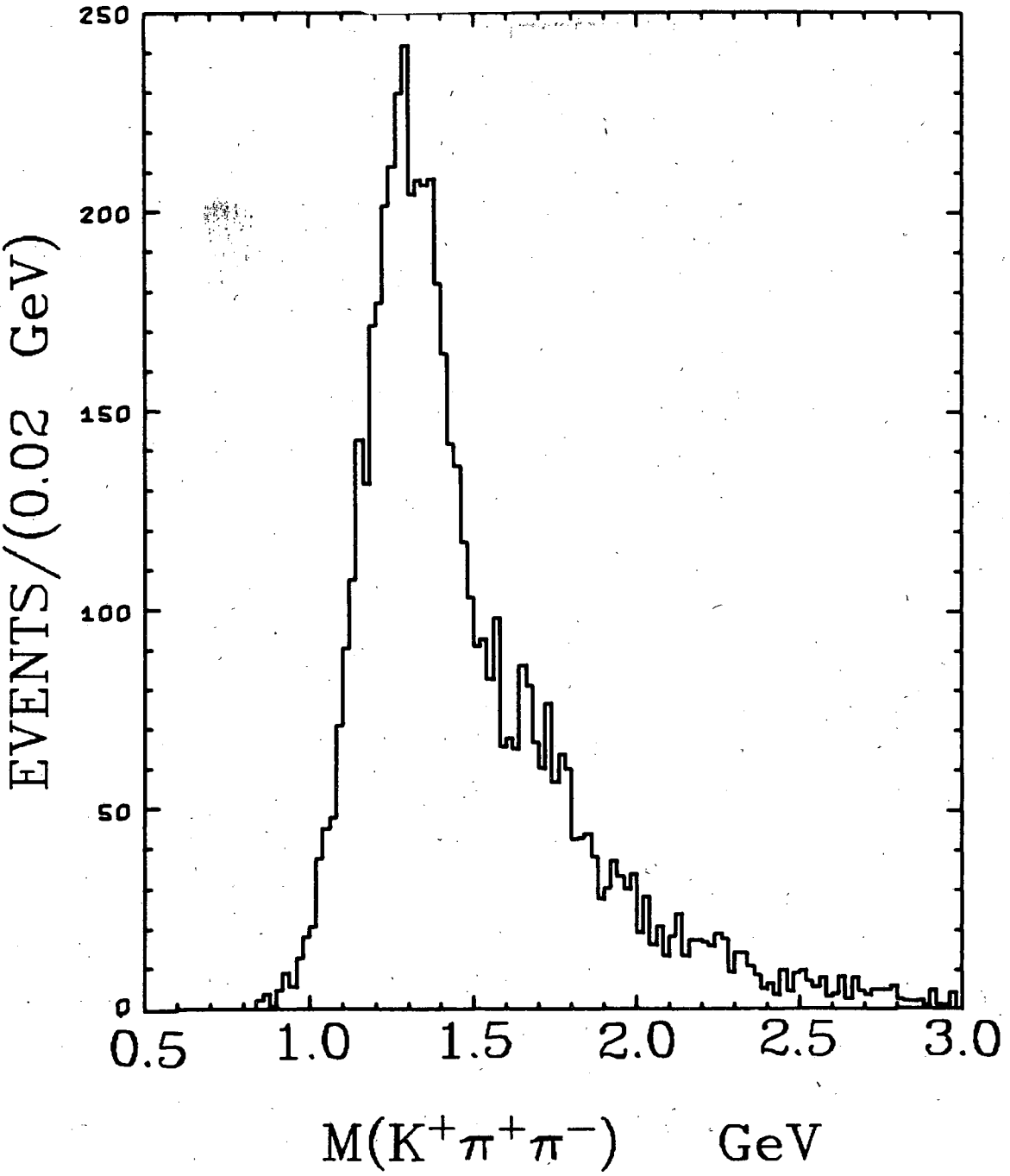

XBL 718-1316

Fig. 7

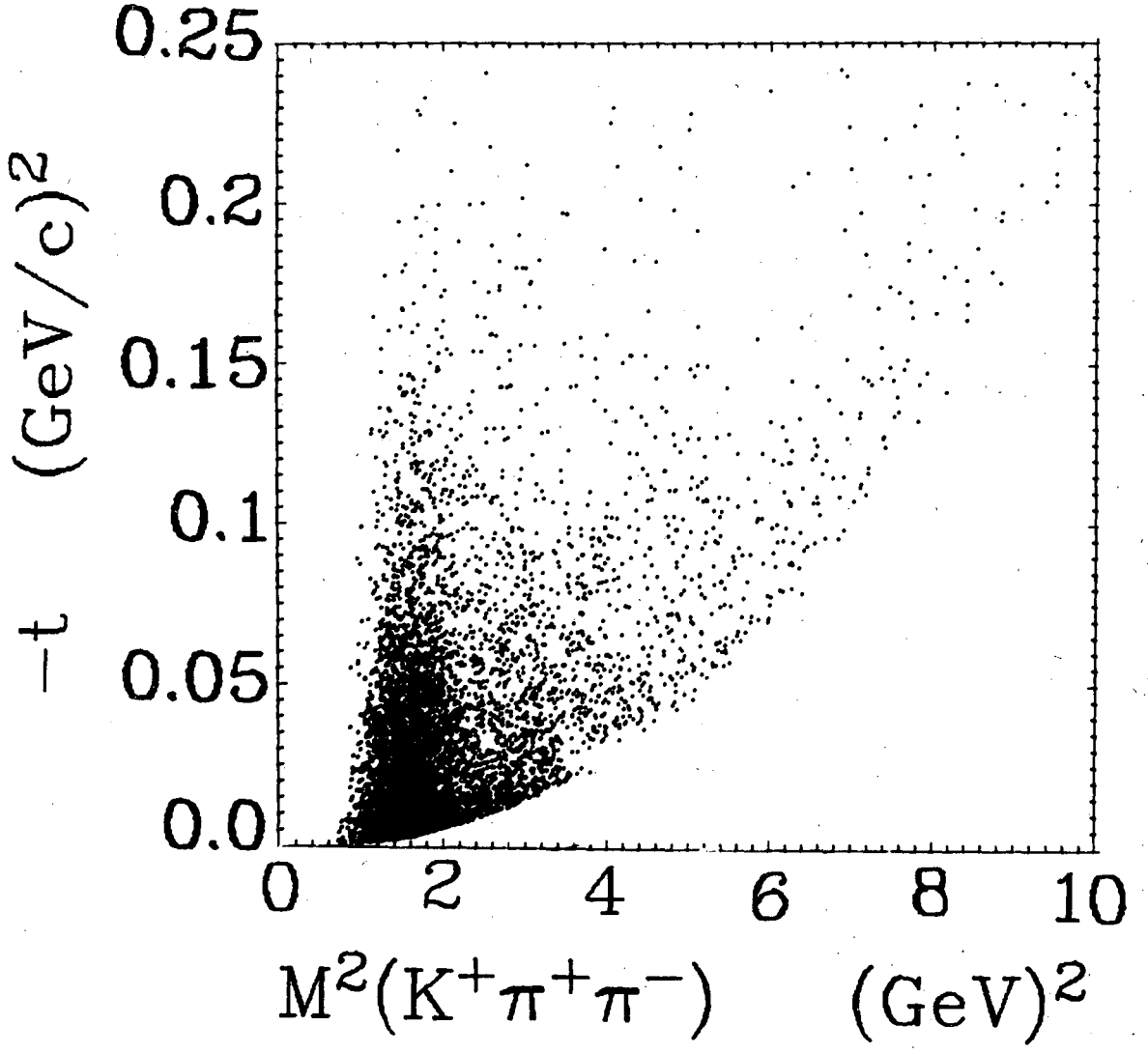

XBL 719-1358

Fig. 8

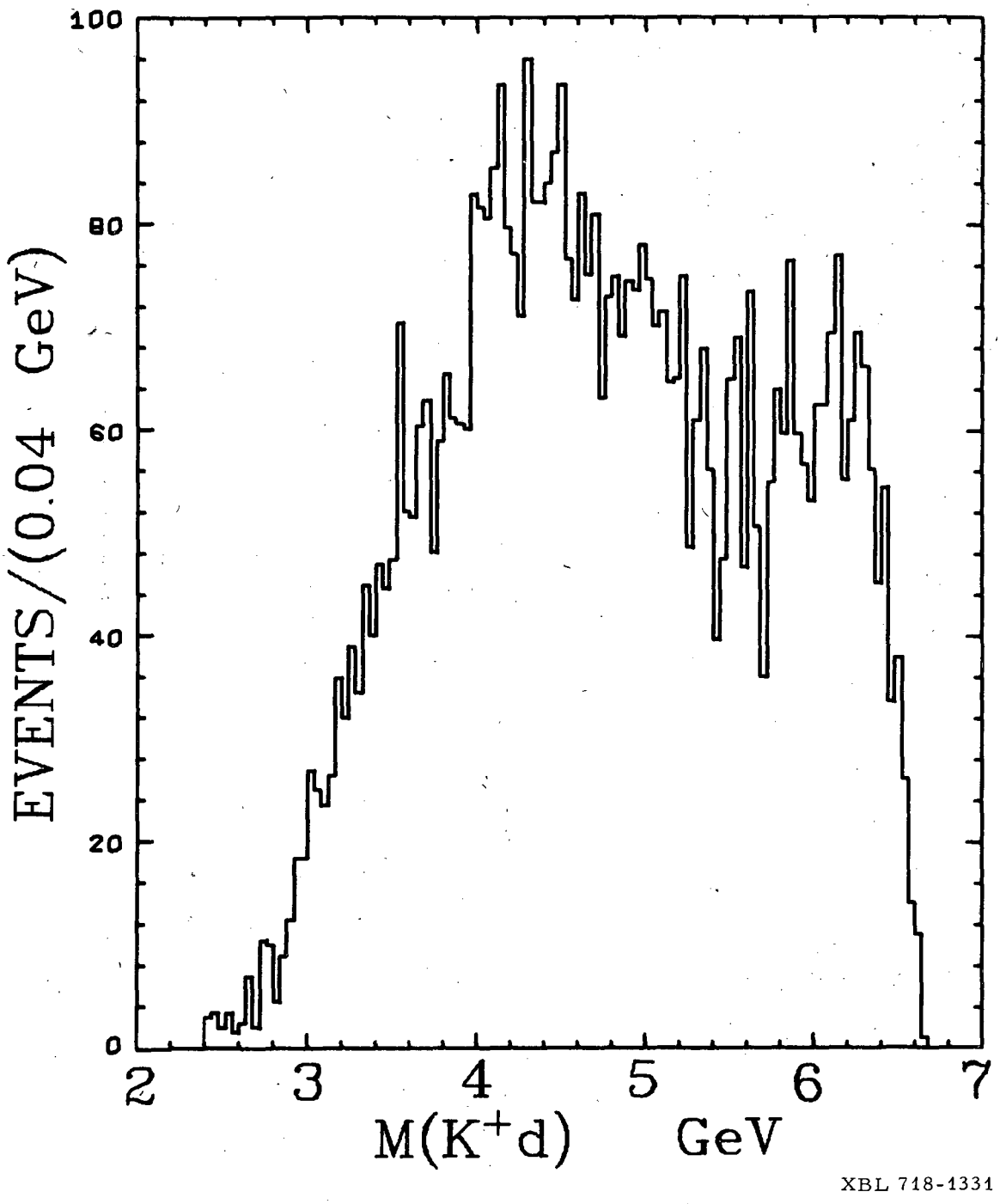

Fig. 9

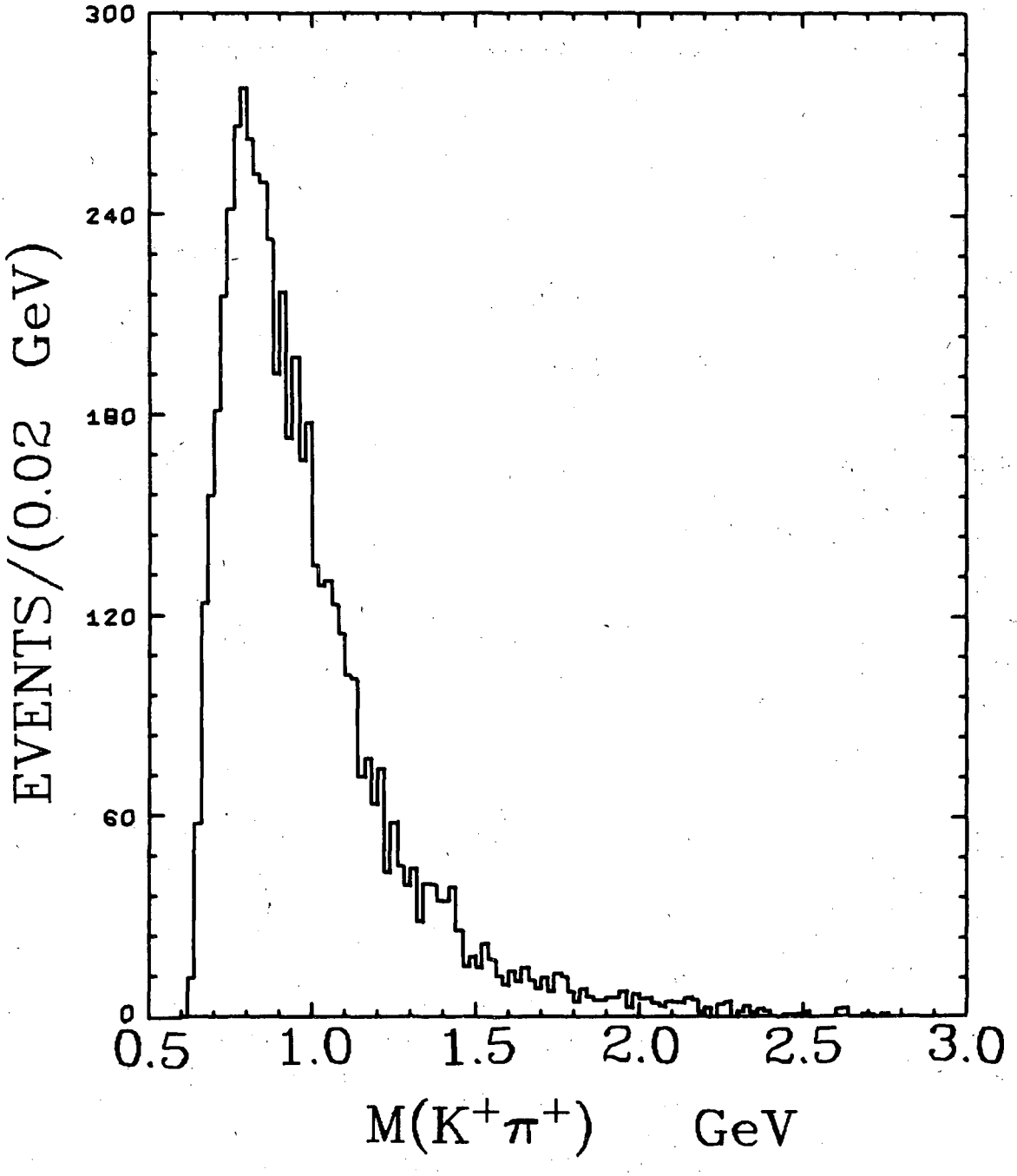

XBL 718-1317

Fig. 10

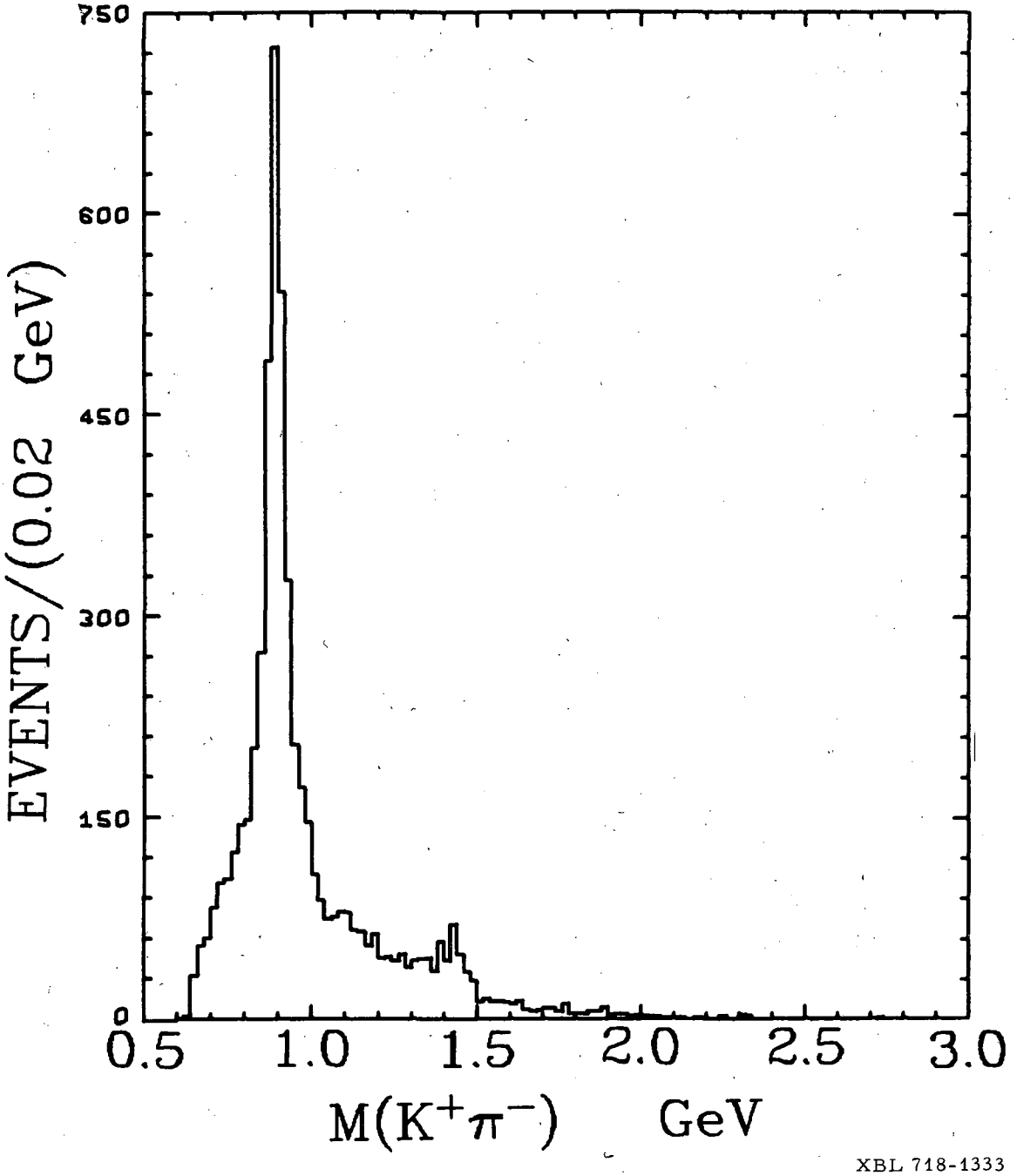
750
600
450
300
150
0
EVENTS/(0.02 GeV)
0.5
1.0
1.5
2.0
2.5
3.0
M(K⁺π⁻) GeV
XBL 718-1333

Fig. 11

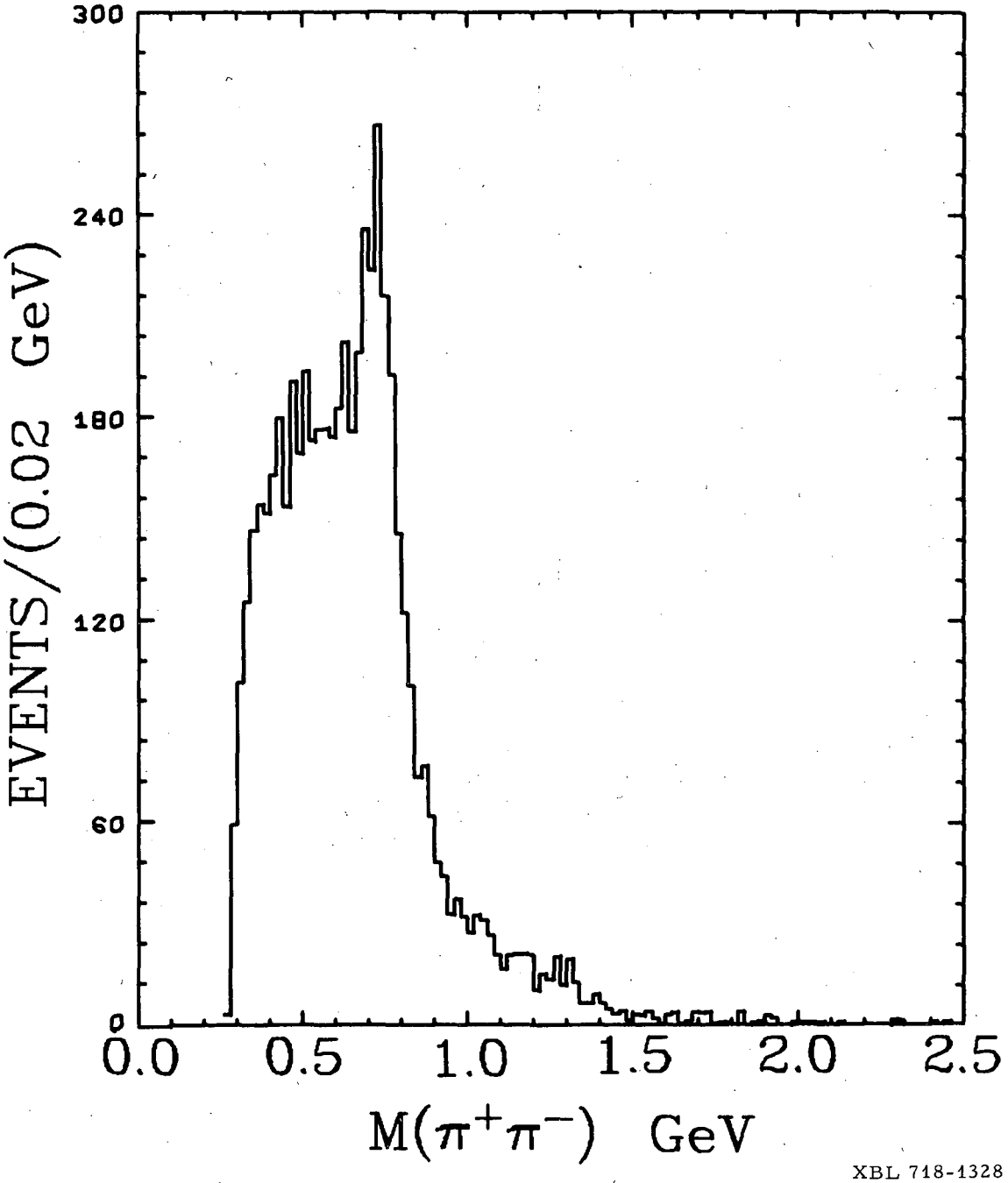

Fig. 12

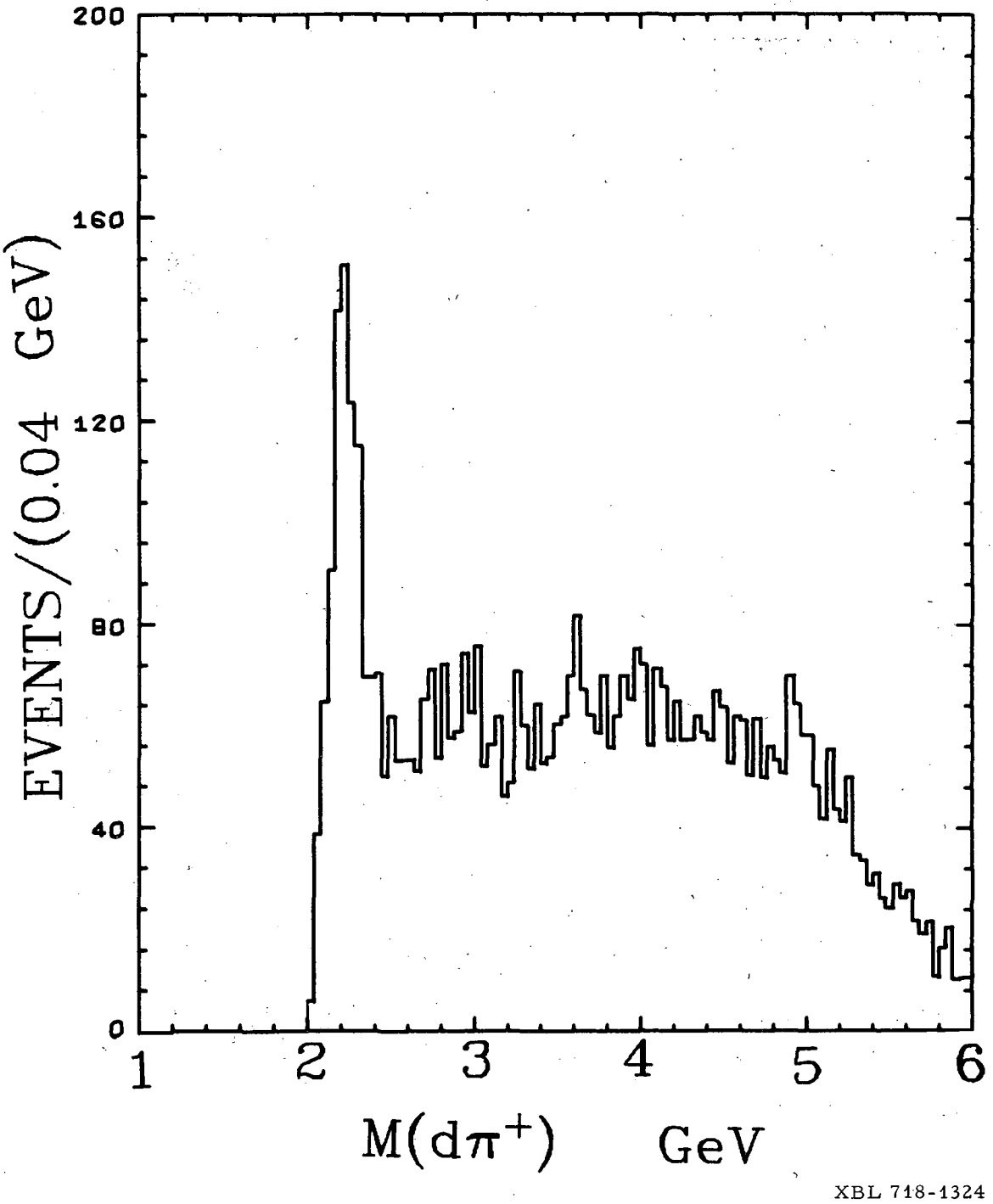

Fig. 13

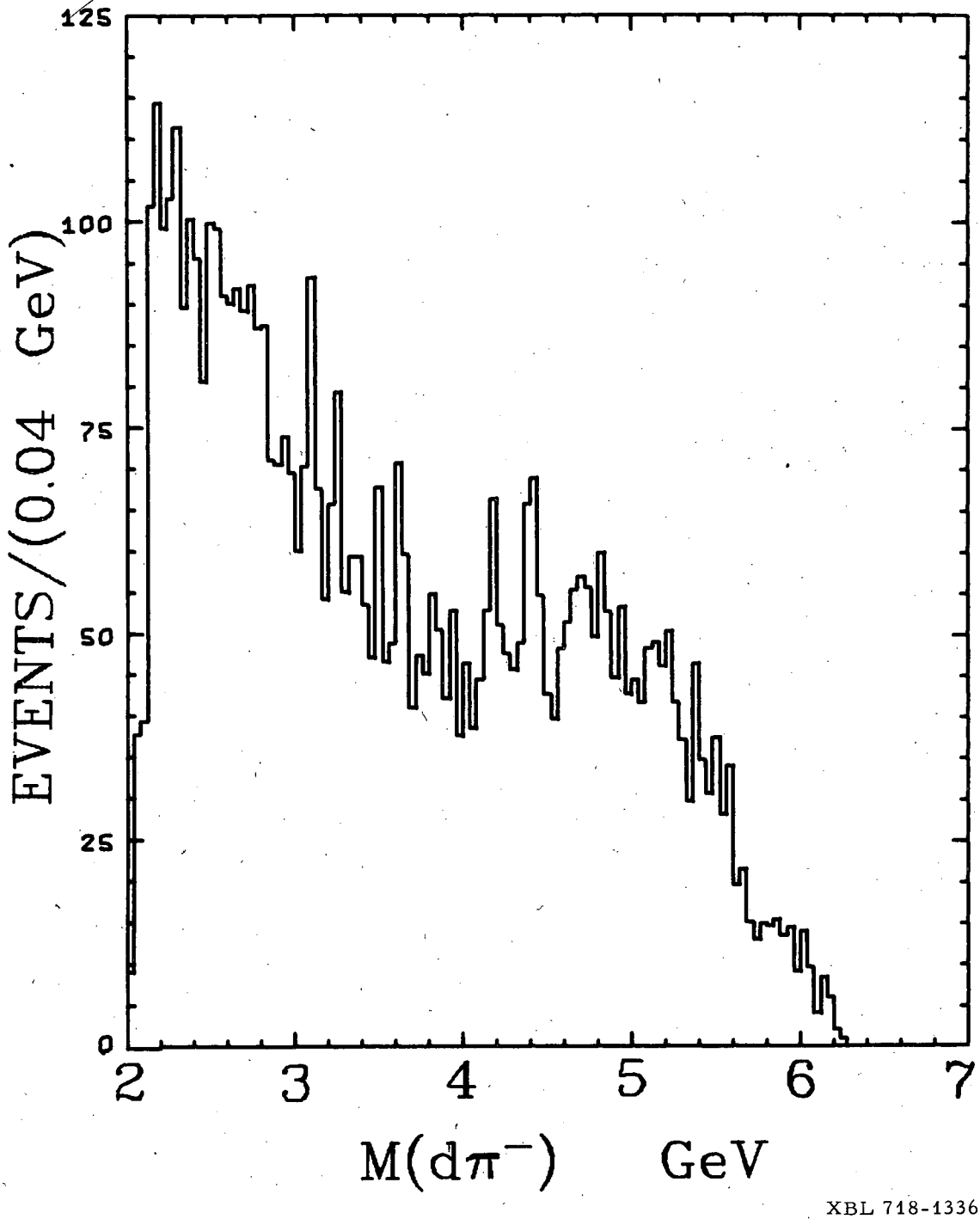

XBL 718-1336

Fig. 14

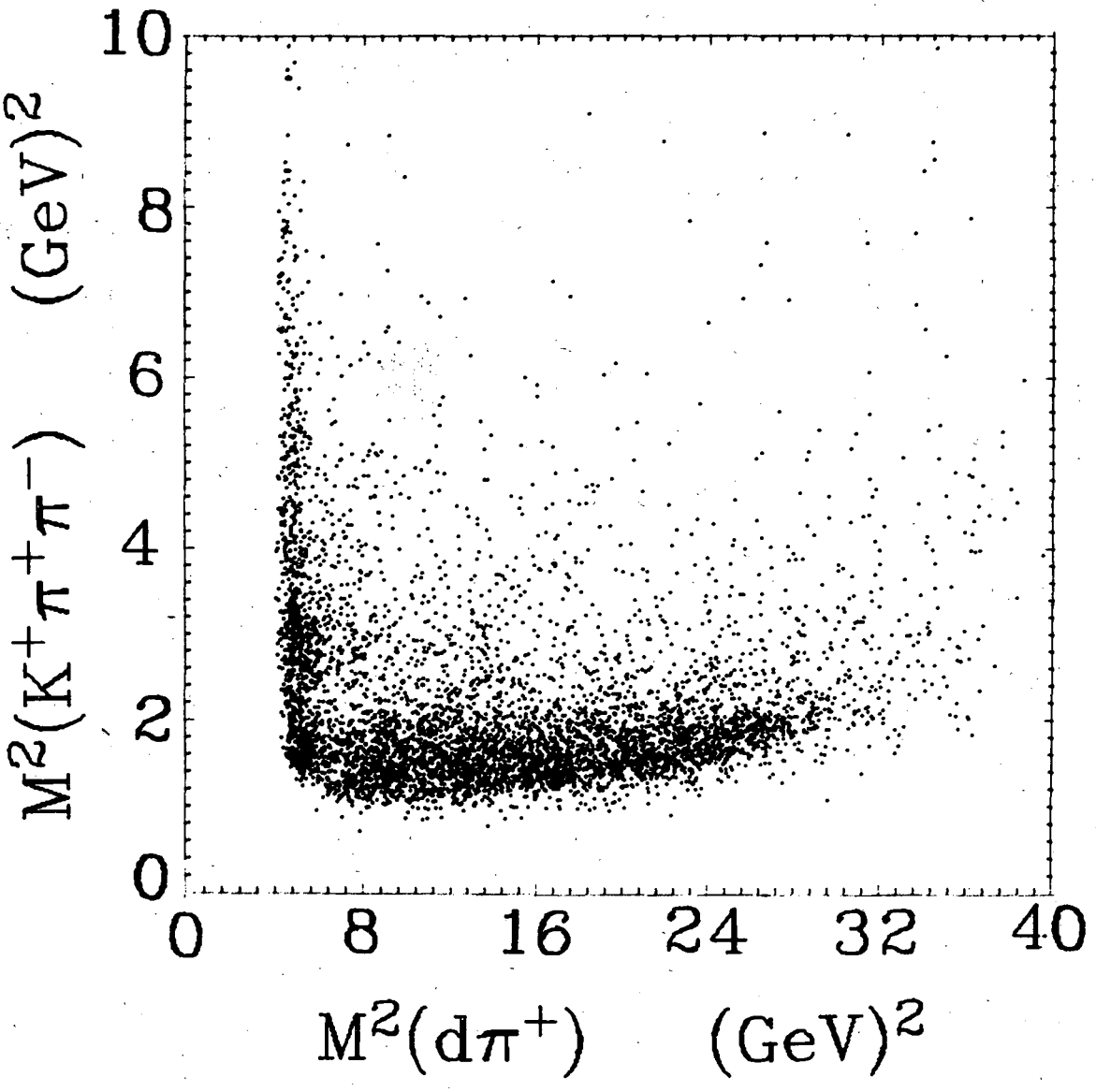

Fig. 15

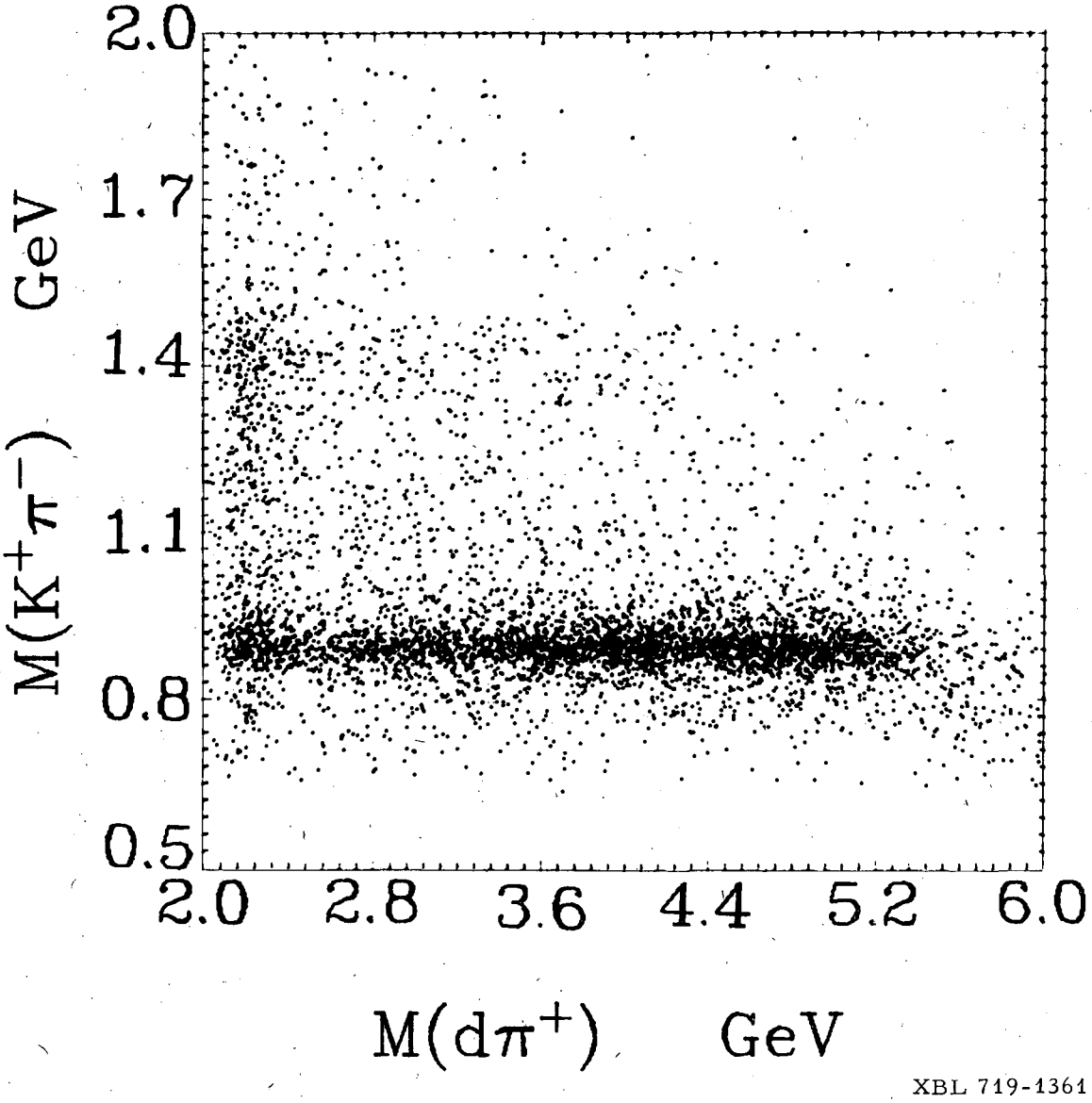

XBL 719-1361

Fig. 16

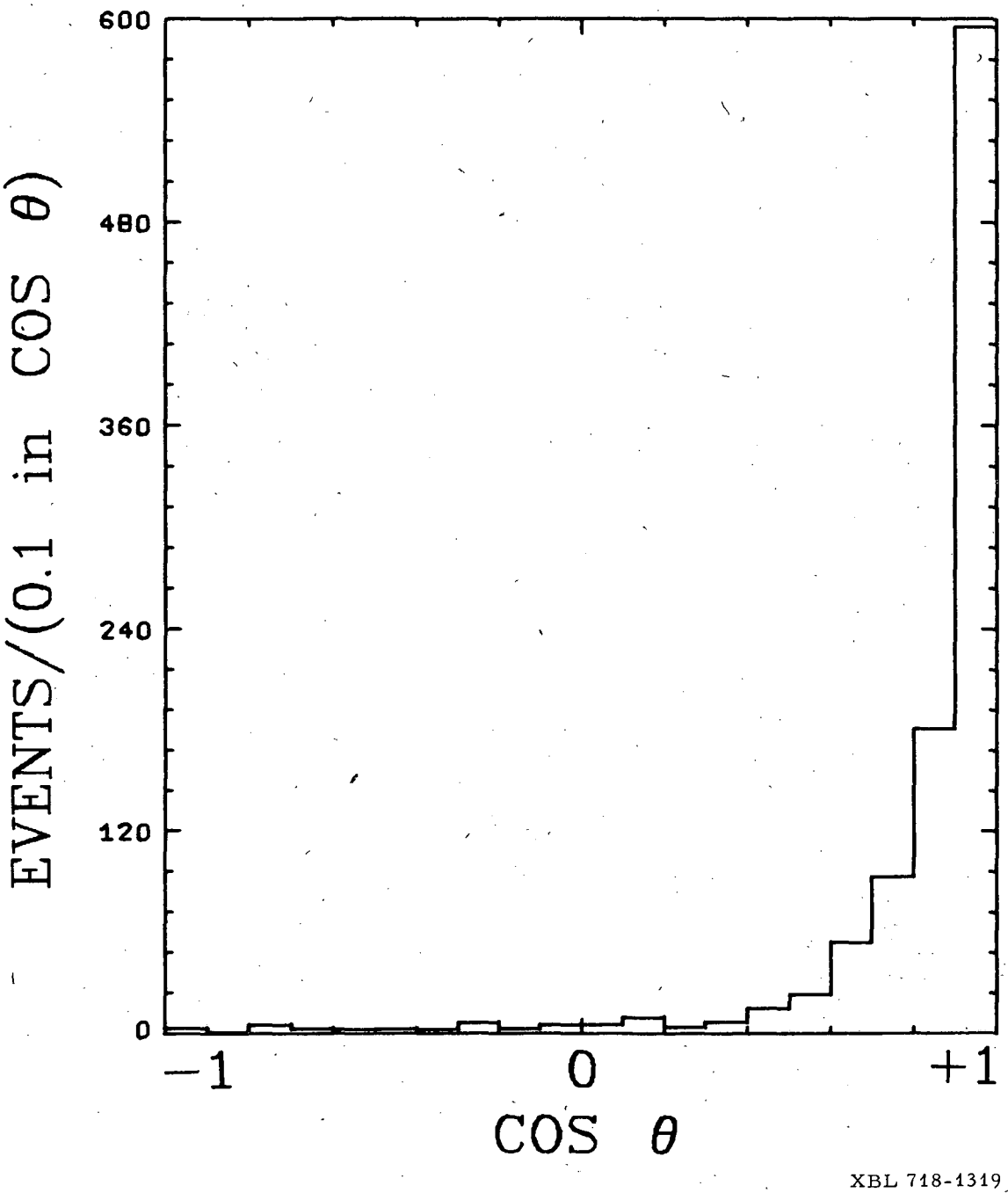

XBL 718-1319

Fig. 17

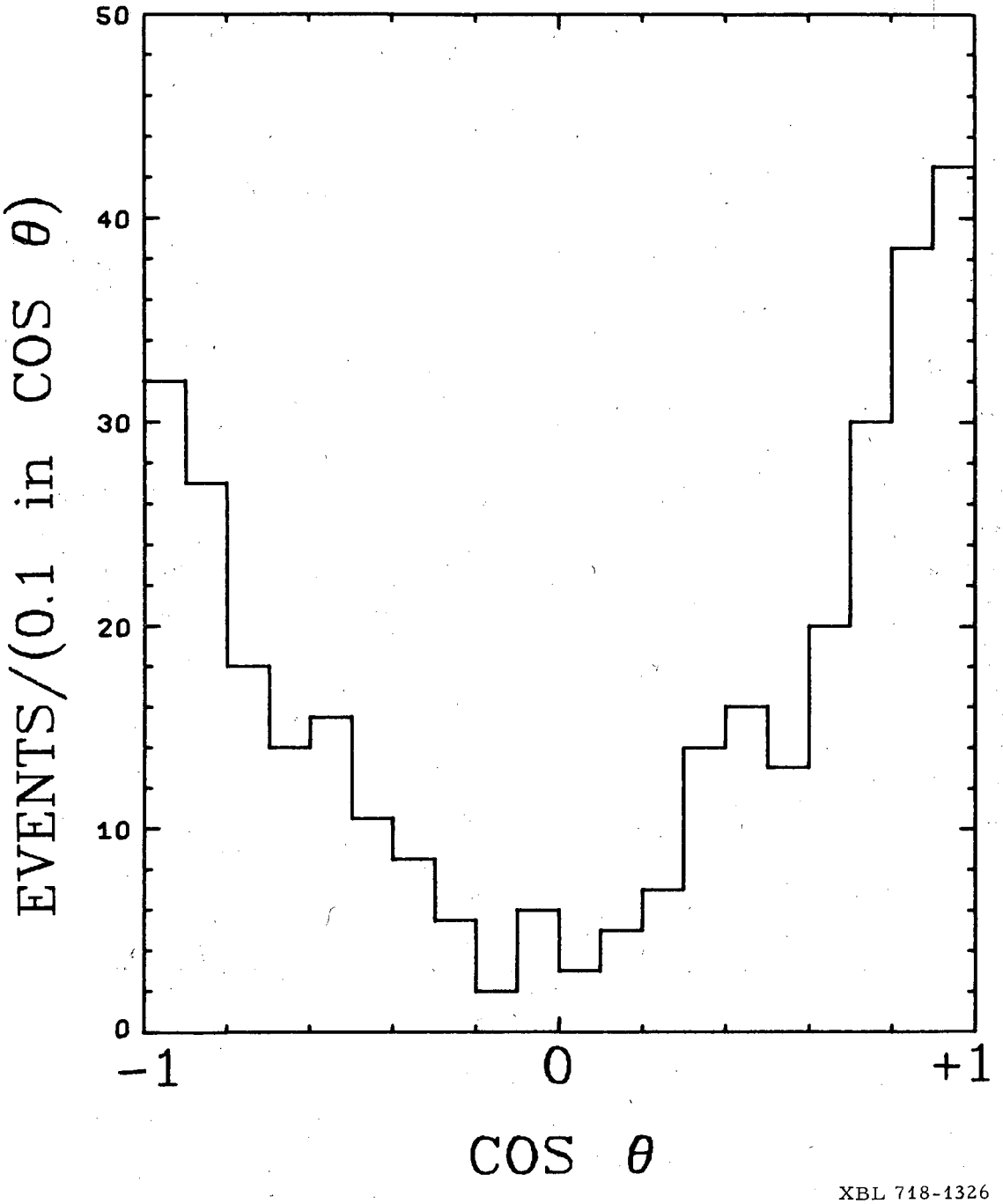

XBL 718-1326

Fig. 18

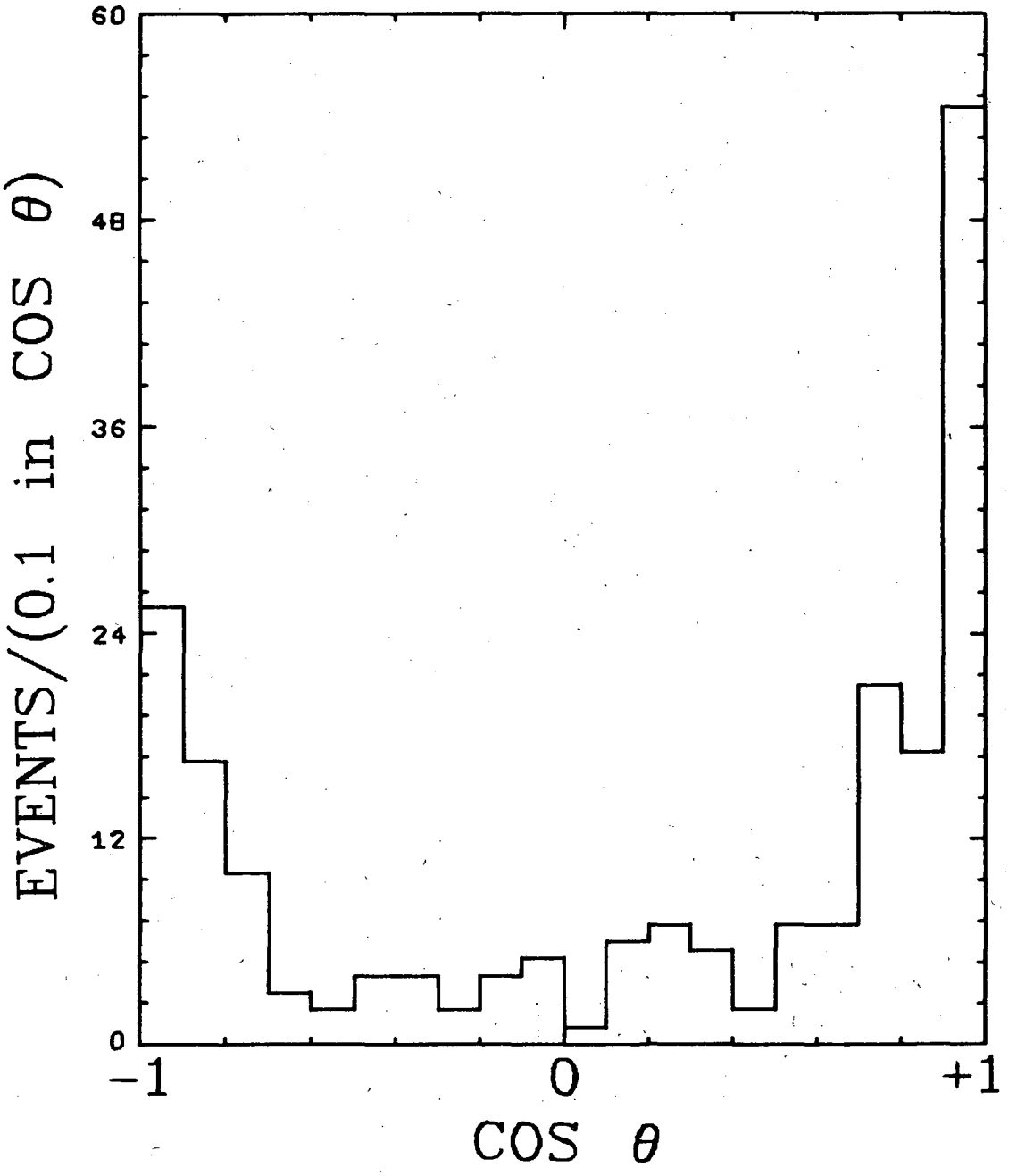

XBL 718-1327

Fig. 19

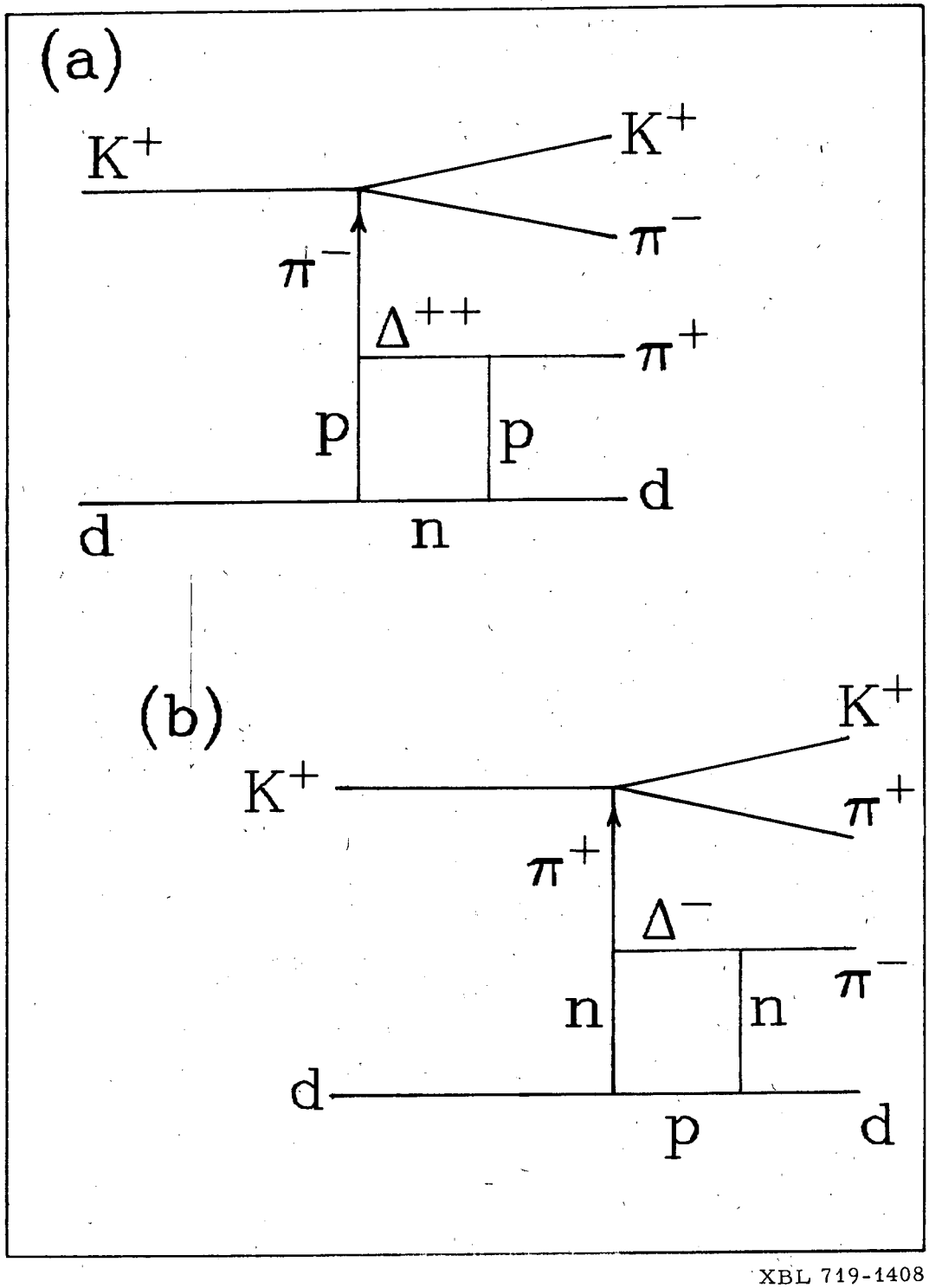

XBL 719-1408

Fig. 20

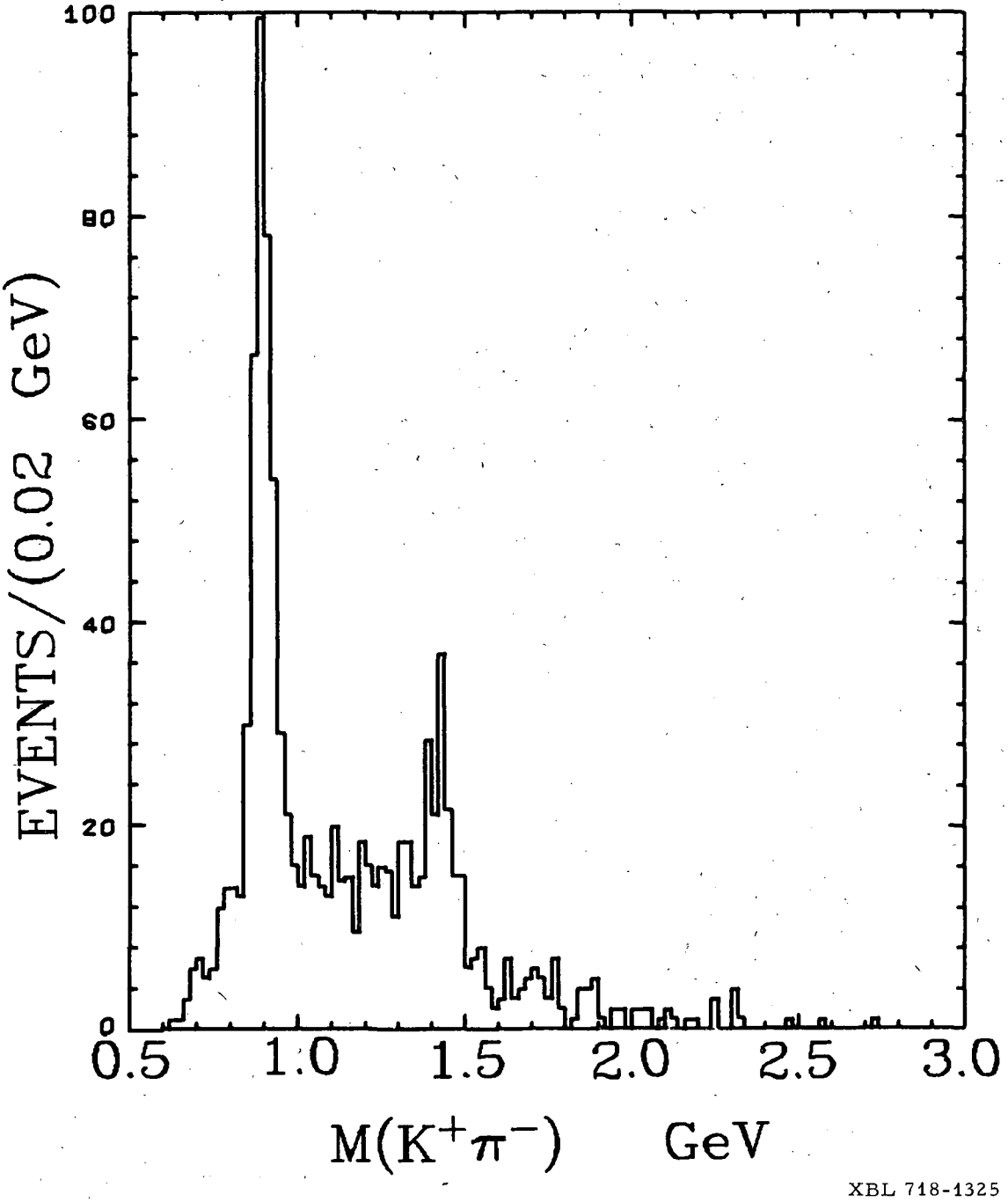
100
80
60
40
20
0
EVENTS/(0.02 GeV)
0.5
1.0
1.5
2.0
2.5
3.0
M(K⁺π⁻) GeV
XBL 718-1325

Fig. 21

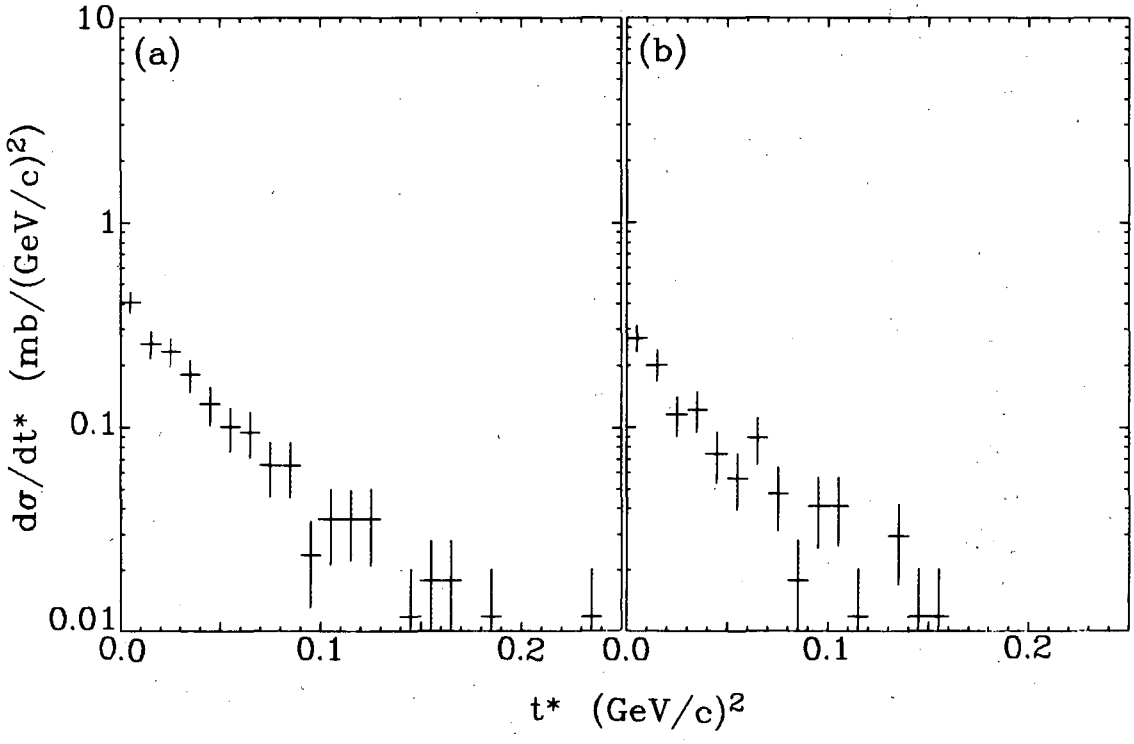

XBL 719-1464

Fig. 22

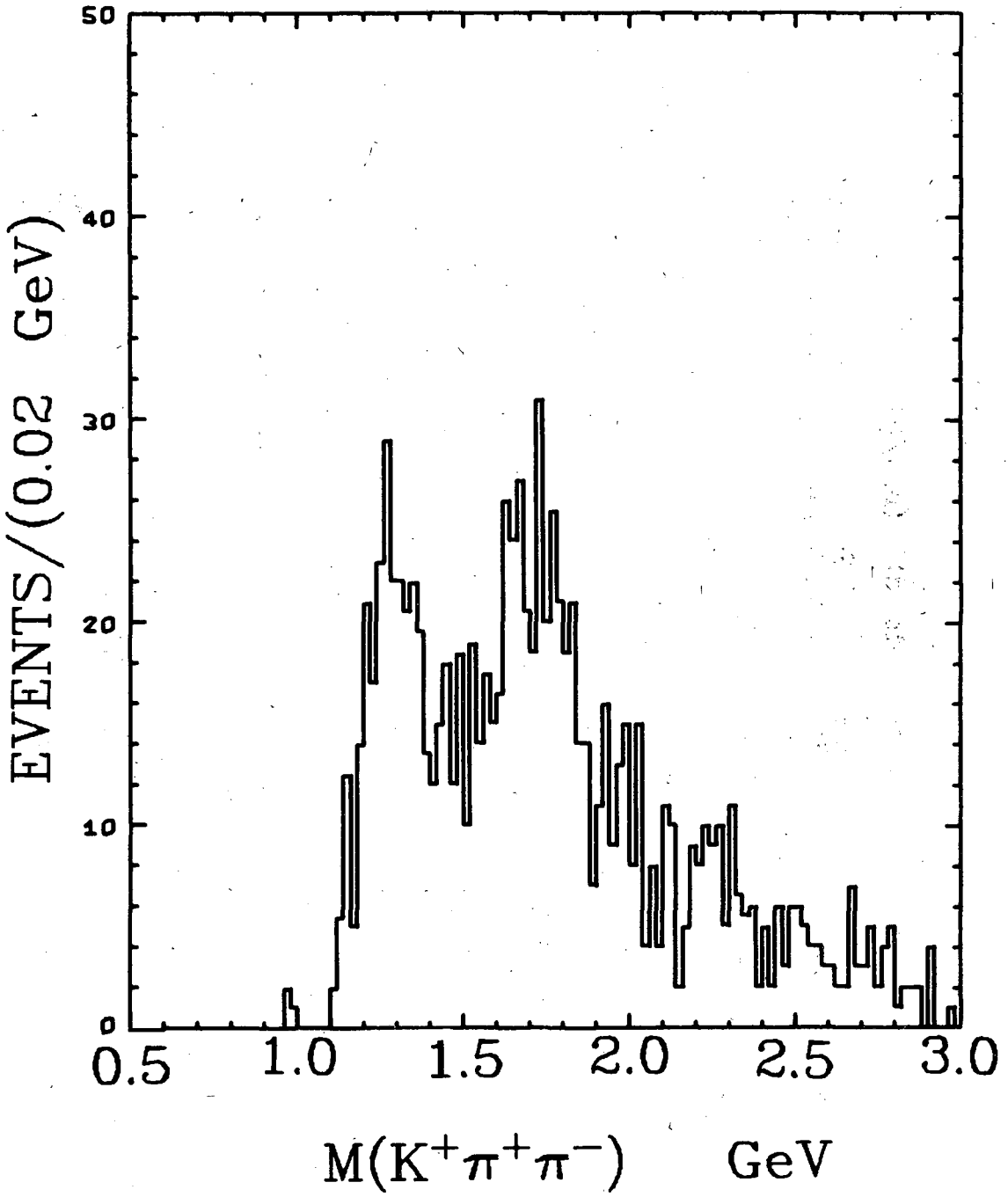
50
40
30
20
10
0
EVENTS/(0.02 GeV)
0.5
1.0
1.5
2.0
2.5
3.0
M(K⁺π⁺π⁻) GeV
XBL 718-1320

Fig. 23

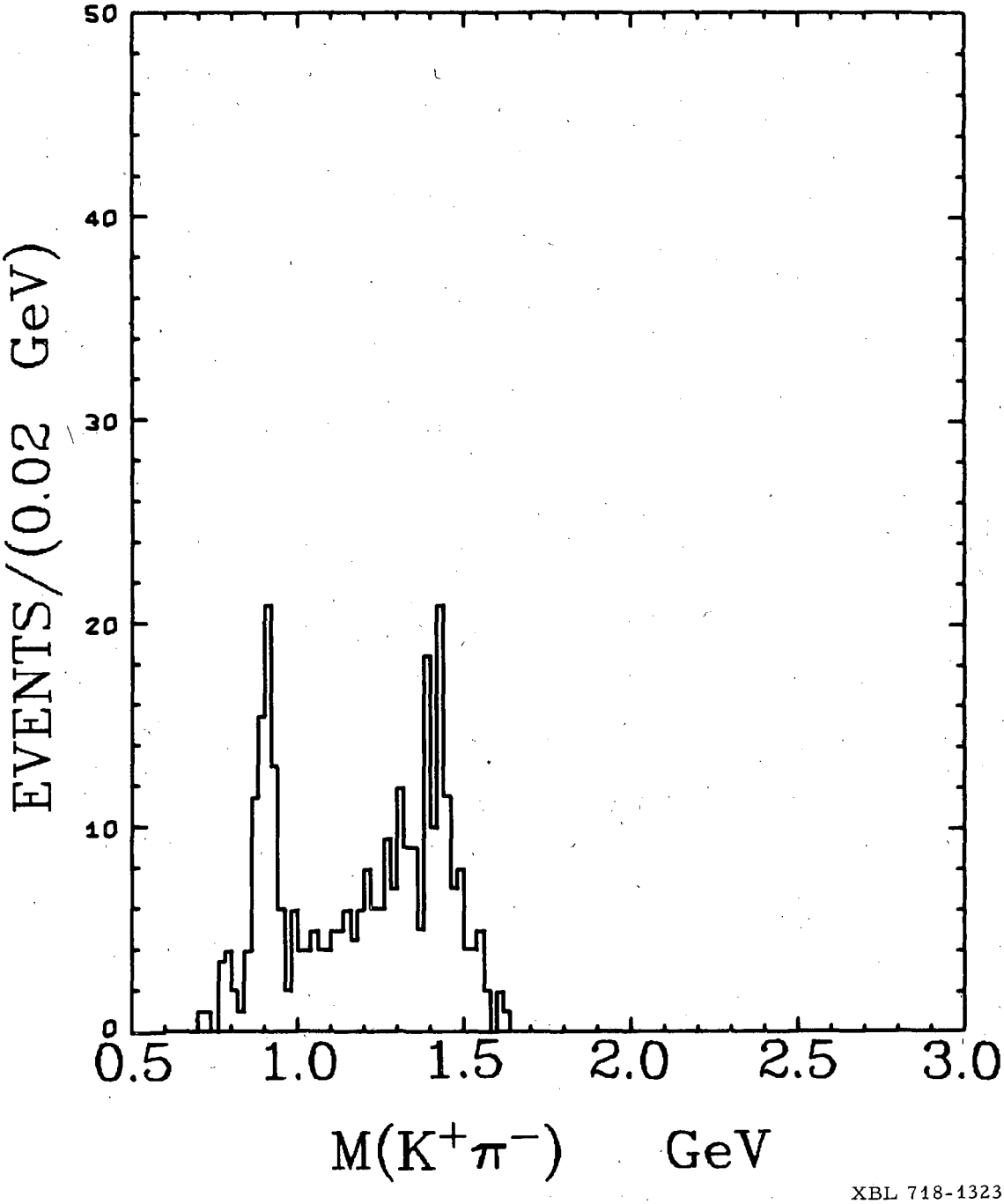

Fig. 24

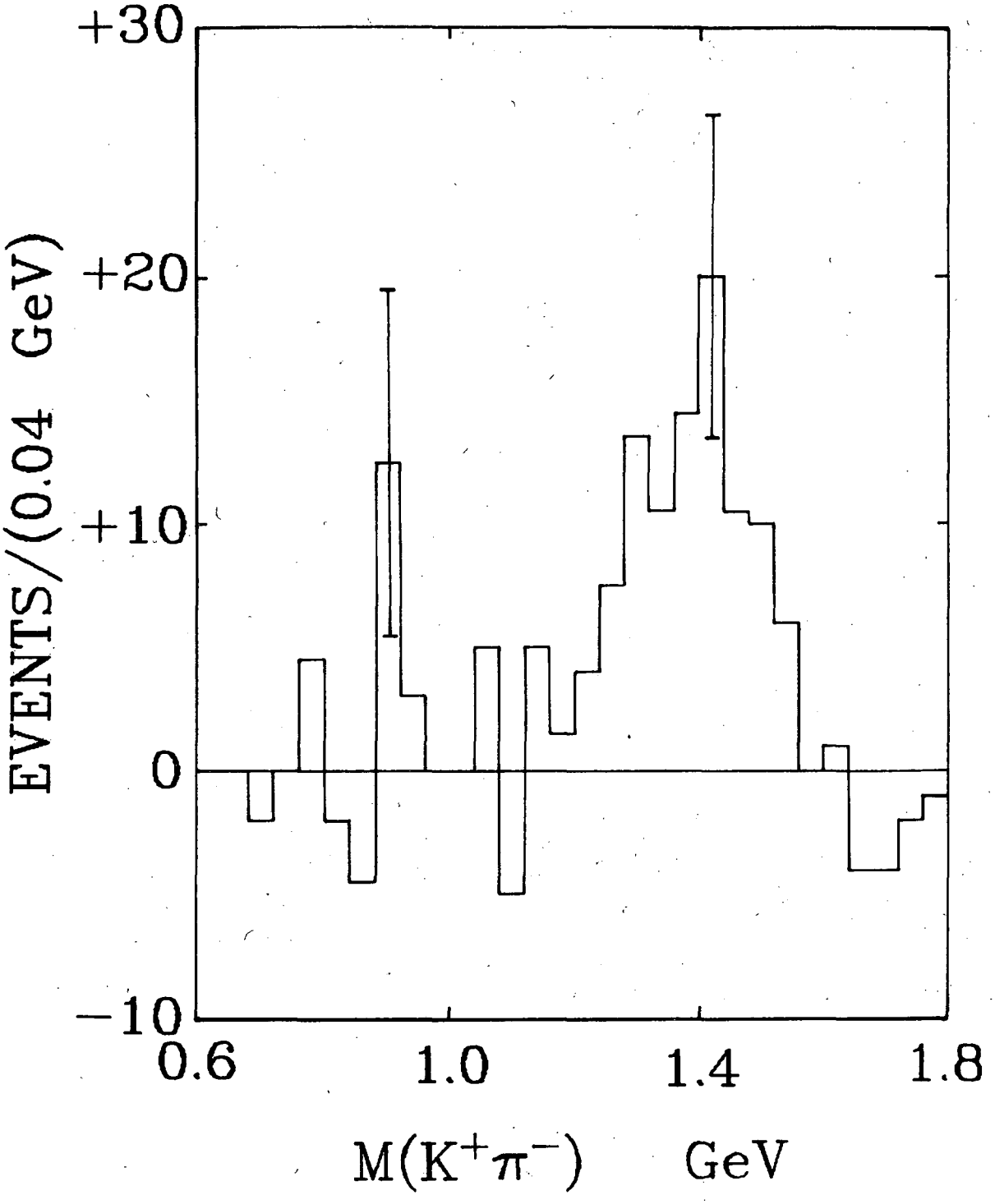

Fig. 25

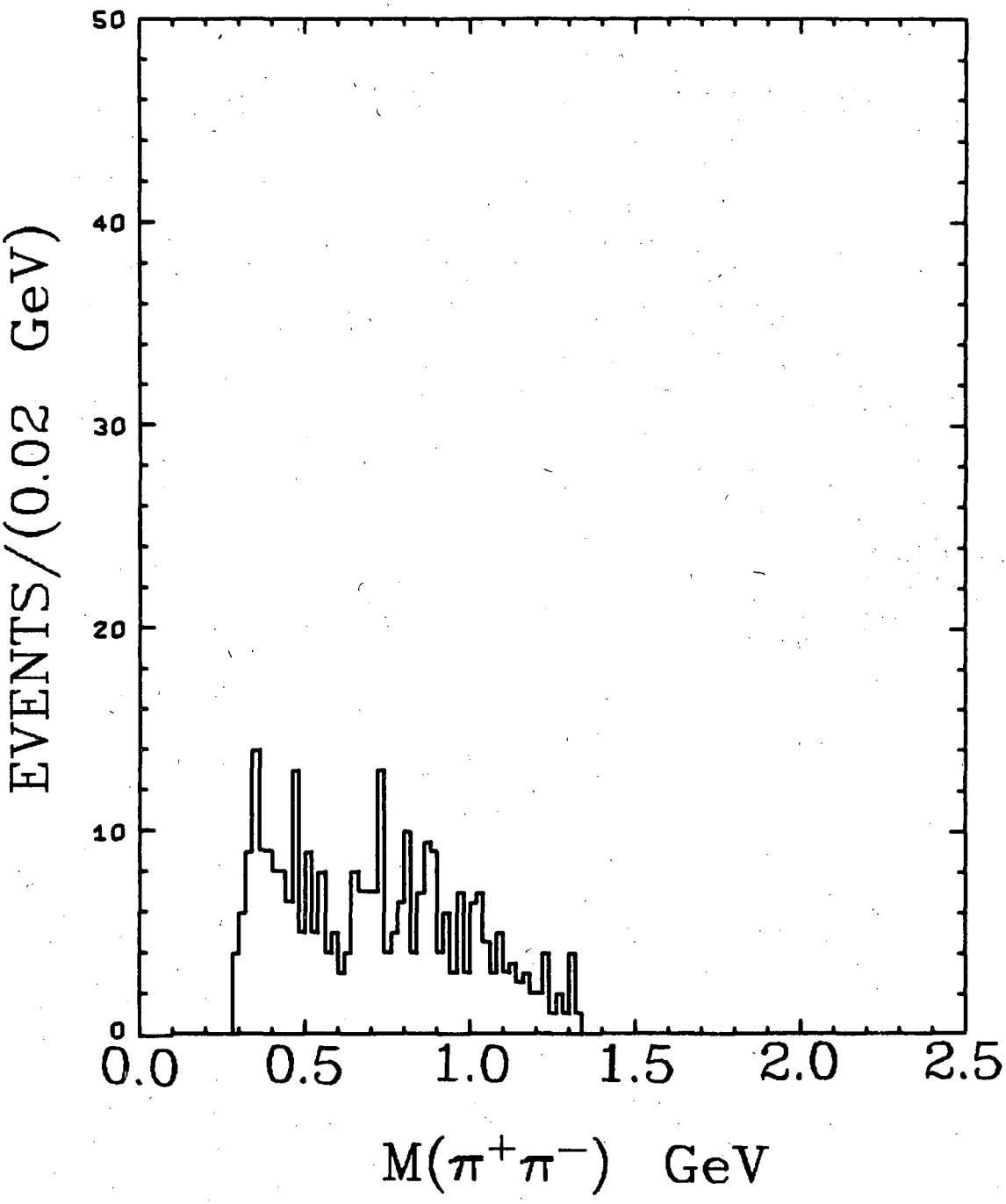

XBL 718-1335

Fig. 26

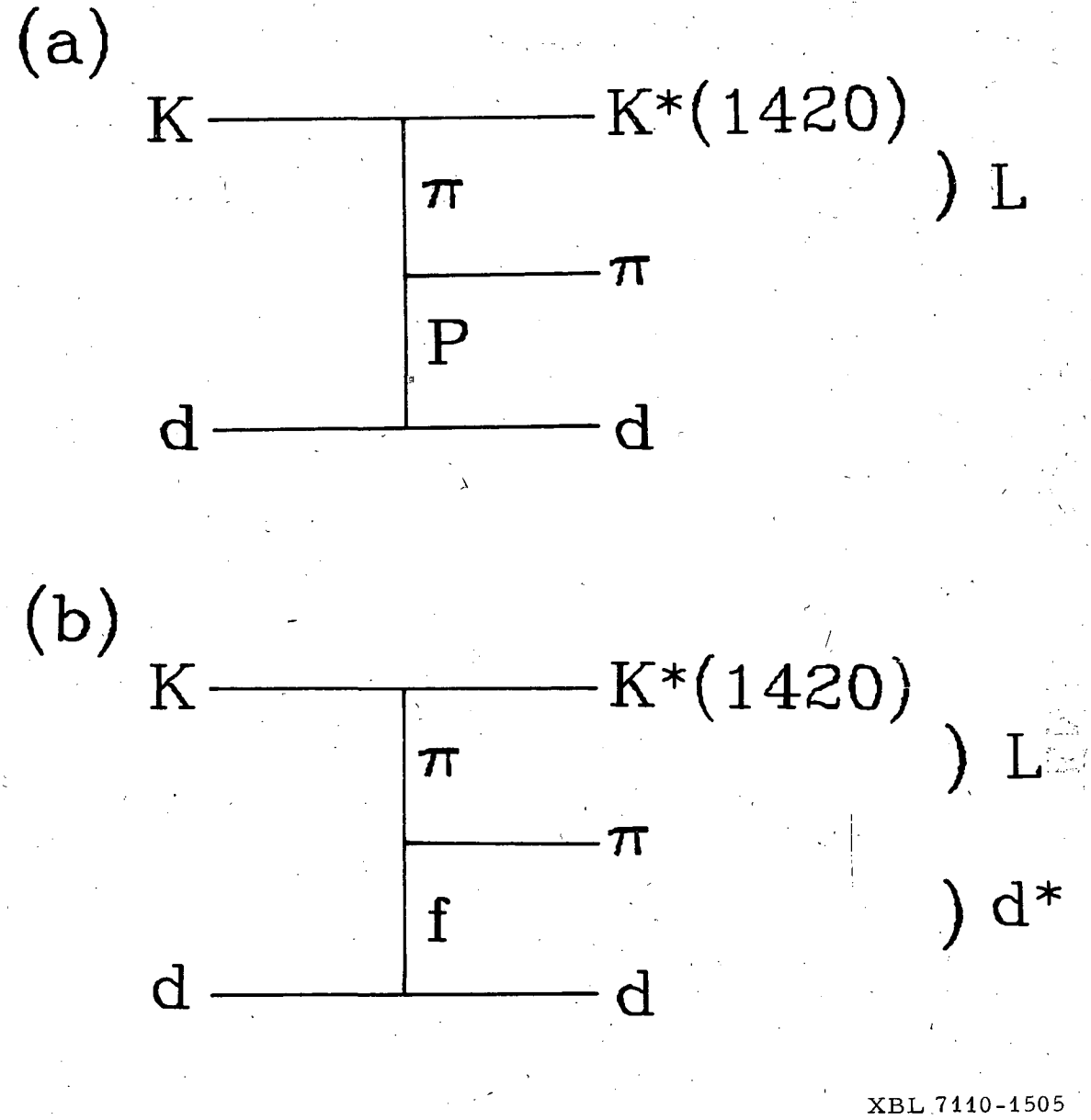

XBL 7110-1505

Fig. 27

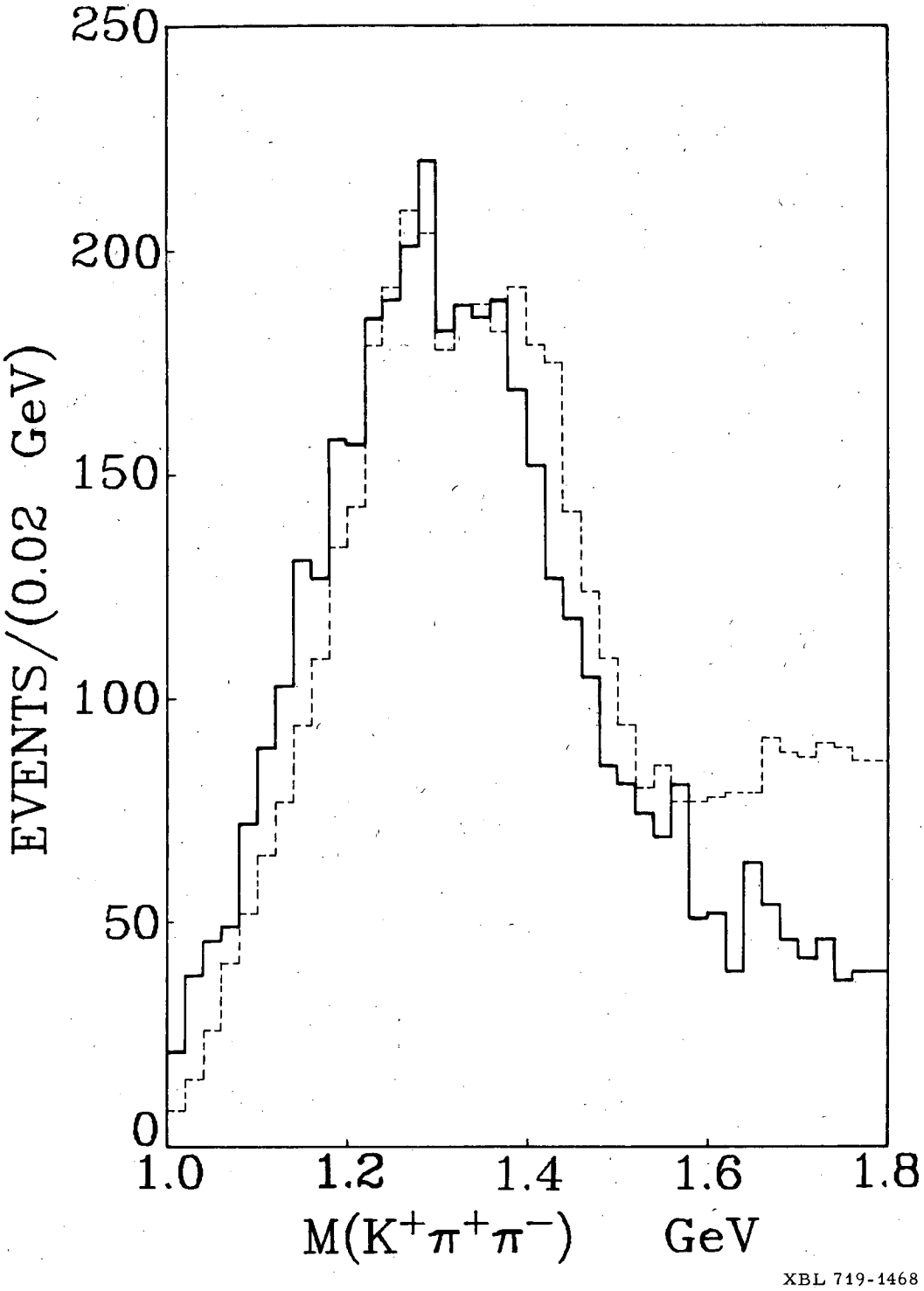

Fig. 28

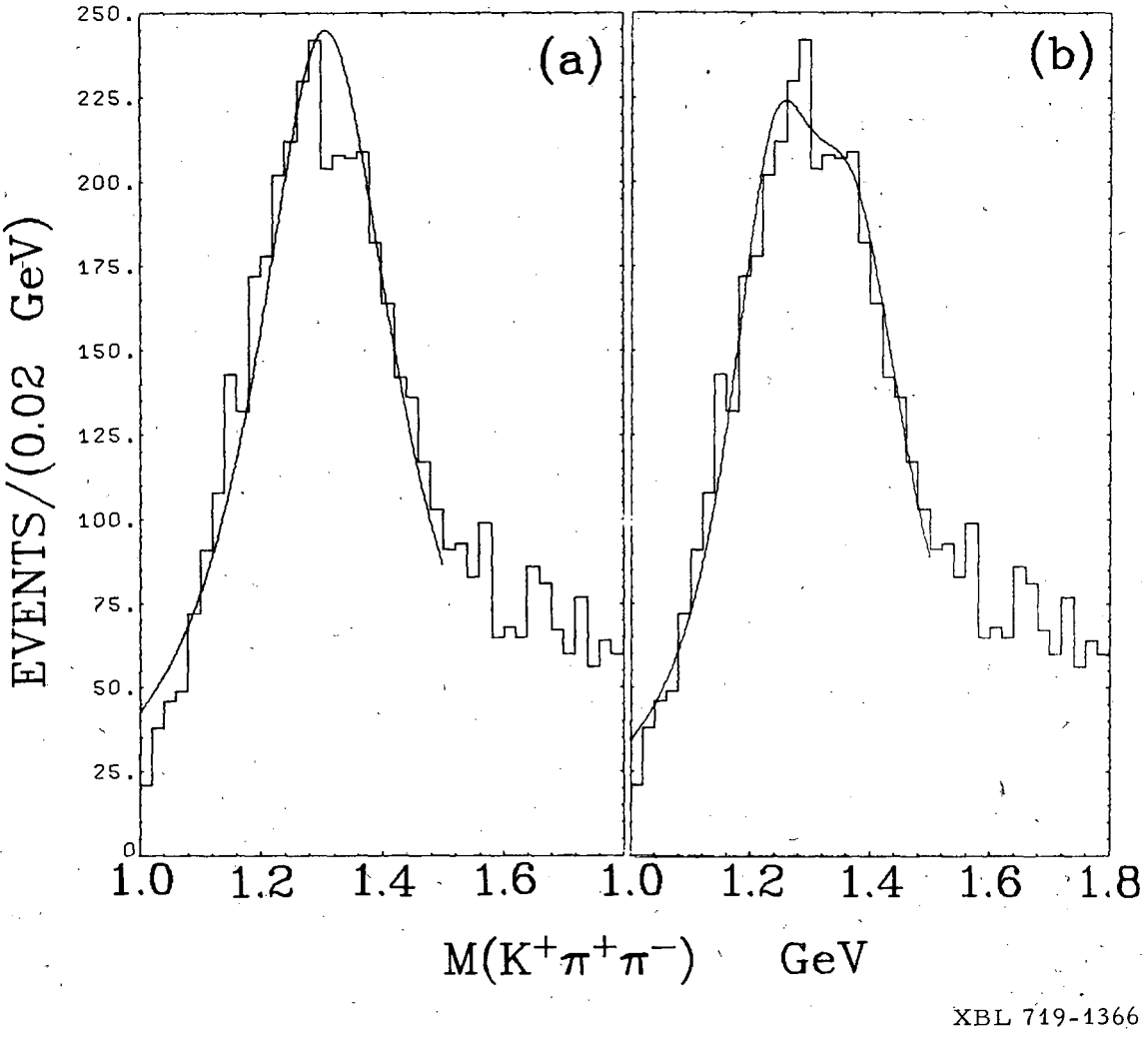

XBL 719-1366

Fig. 29

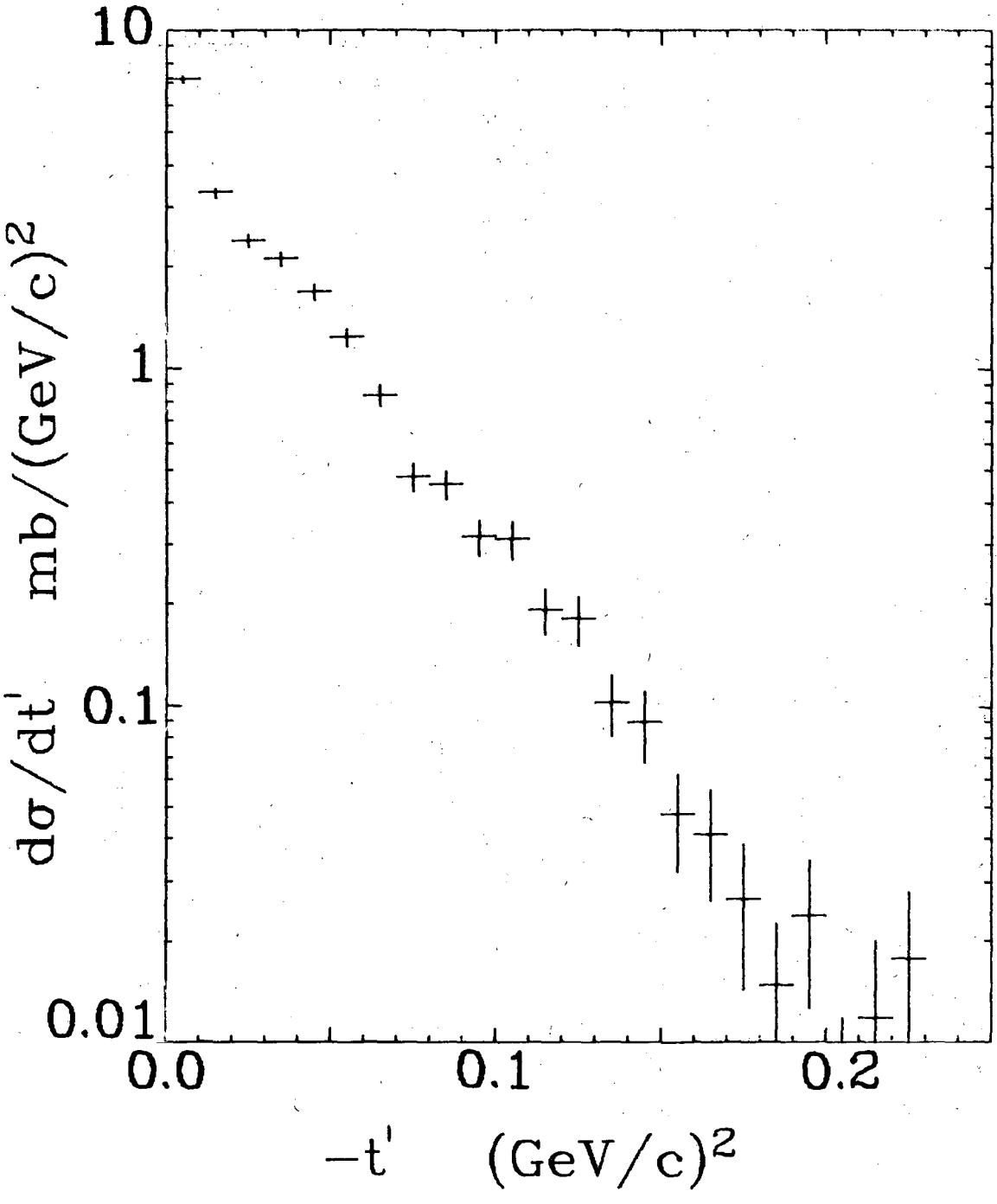

XBL 719-1346

Fig. 30

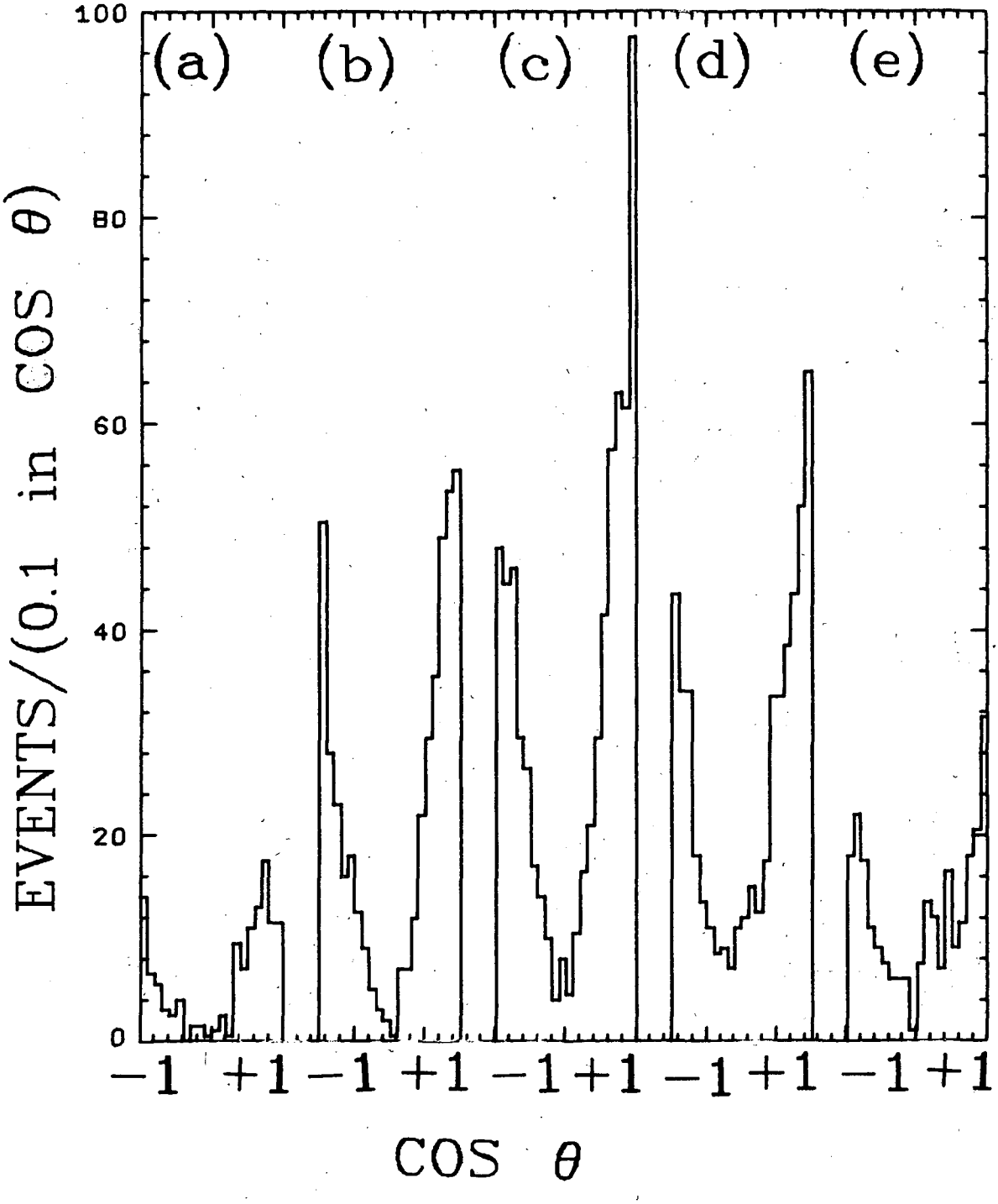

XBL 719-1351

Fig. 31

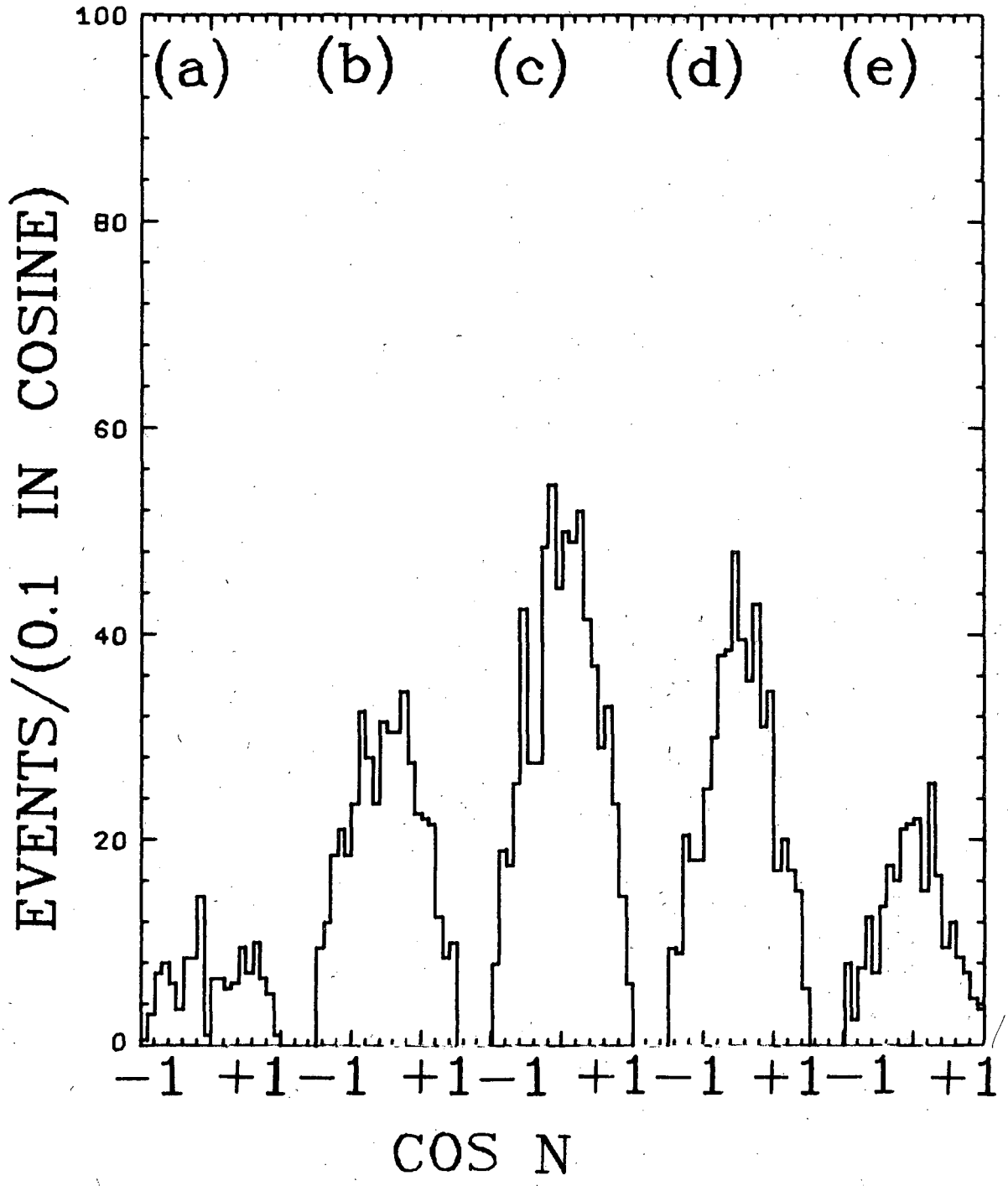

XBL 719-1352

Fig. 32

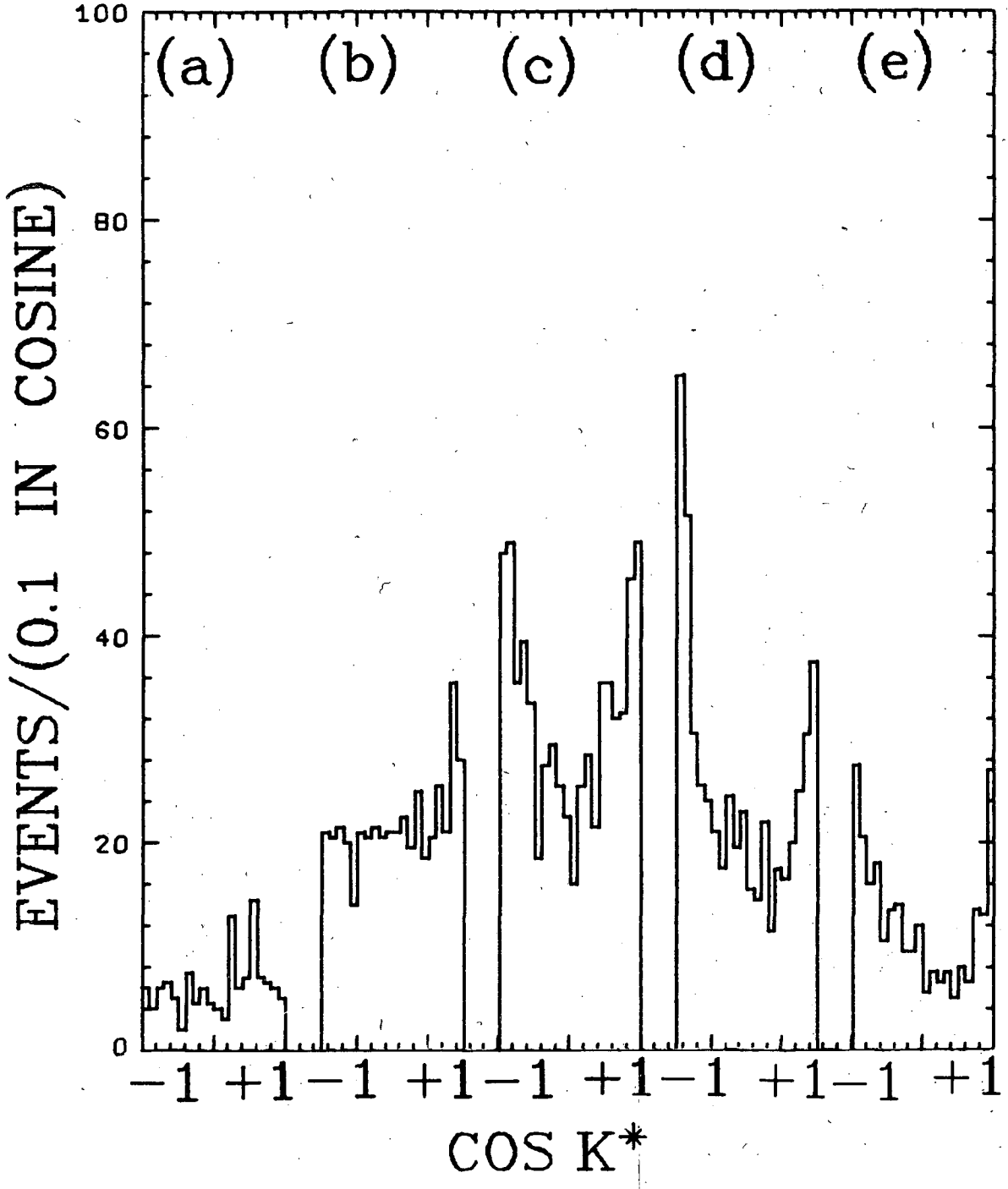

XBL 719-1354

Fig. 33

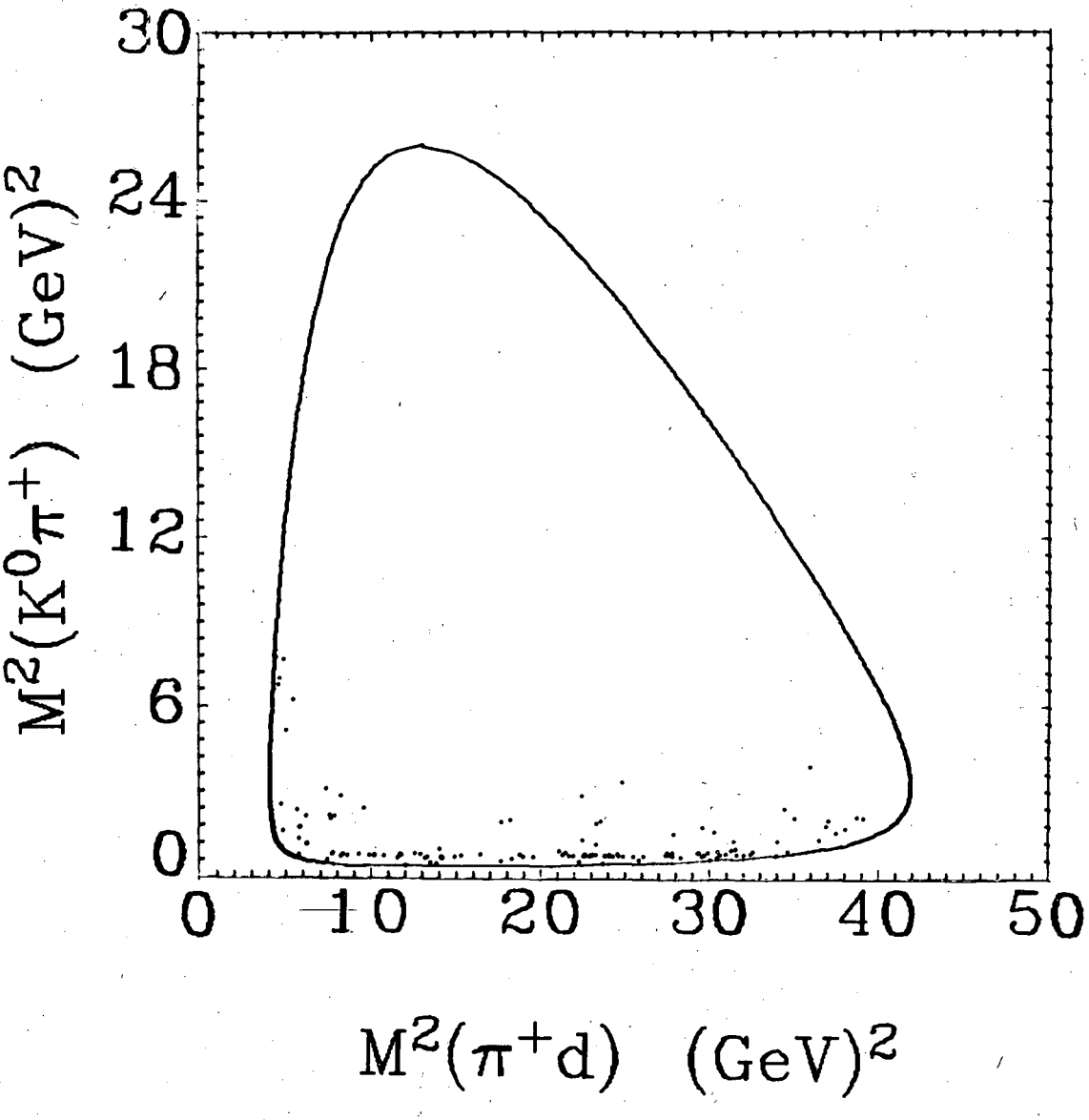

XBL 719-1359

Fig. 34

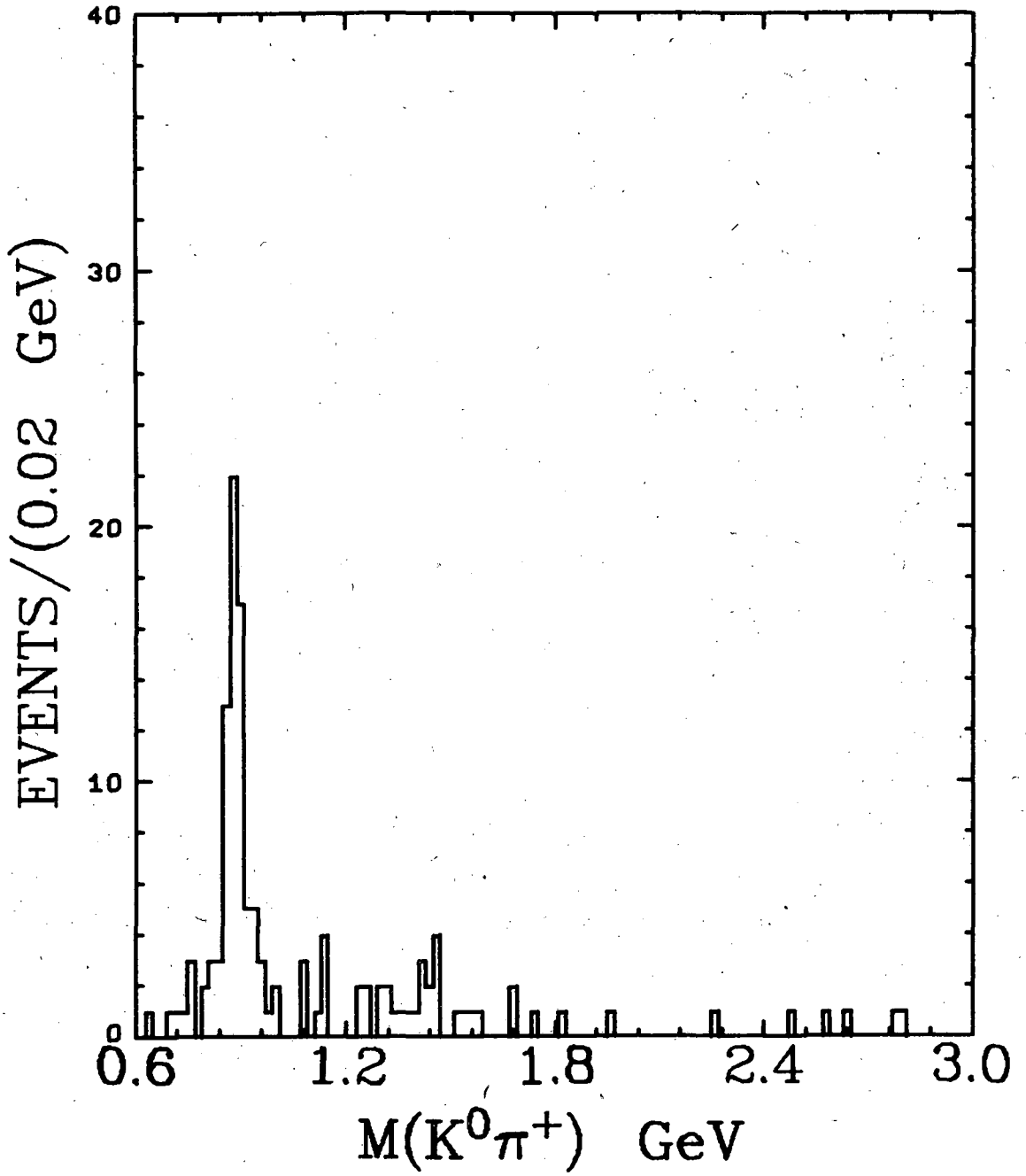

Fig. 35

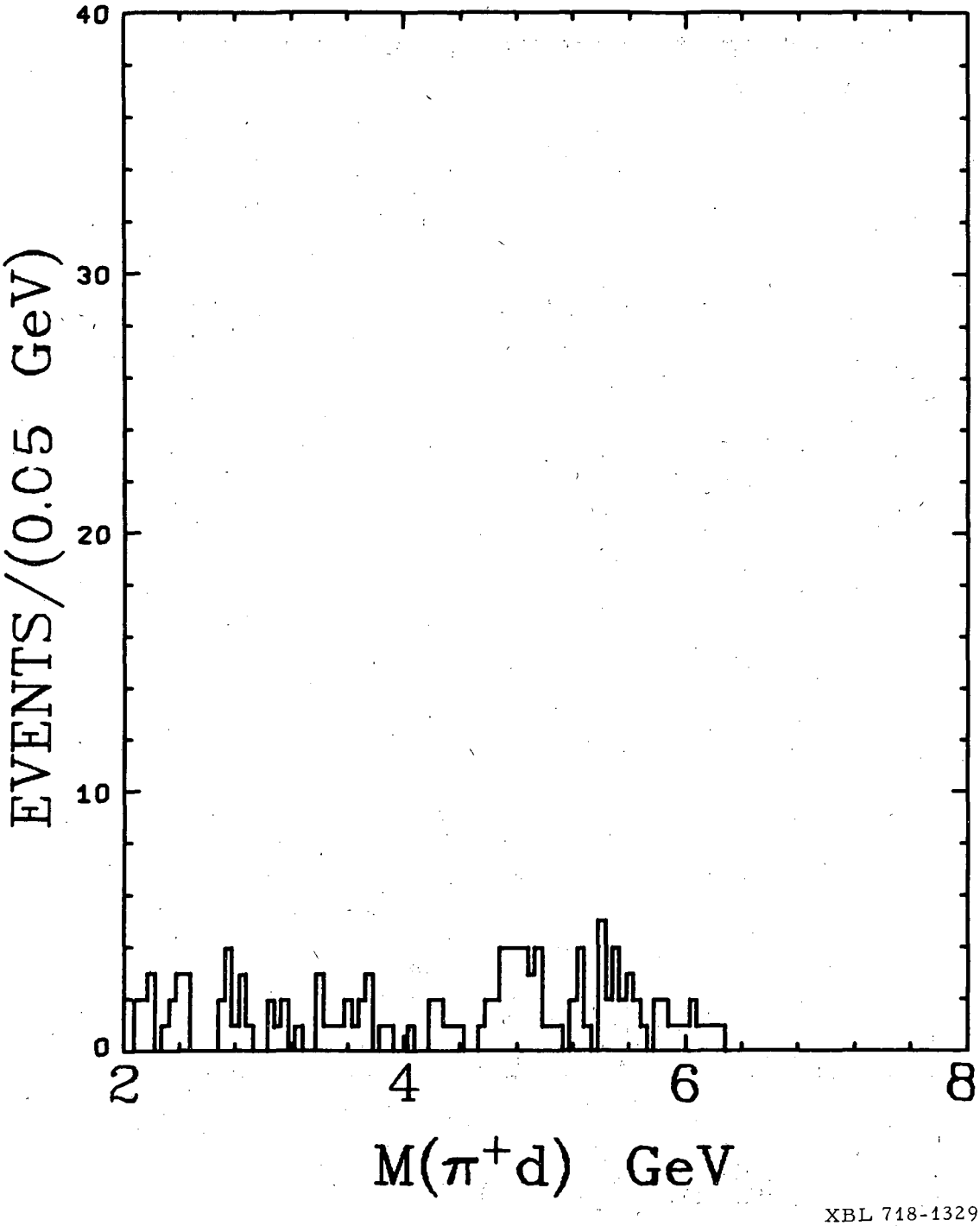

XBL 718-1329

Fig. 36

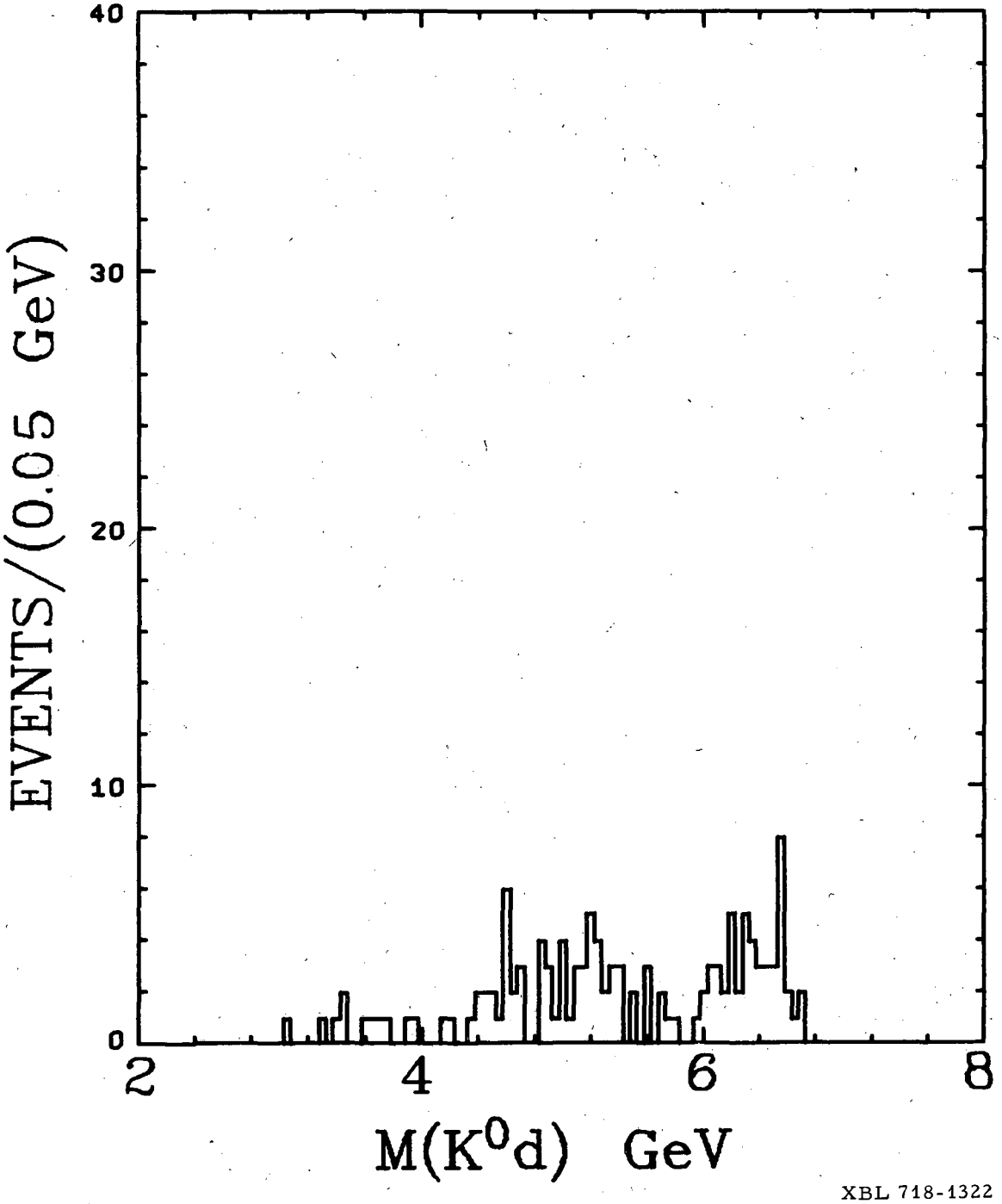

Fig. 37

TECHNICAL INFORMATION DIVISION
LAWRENCE BERKELEY LABORATORY
UNIVERSITY OF CALIFORNIA
BERKELEY, CALIFORNIA 94720